Spectro-electrochemical toolbox for monitoring and controlling quinone-mediated redox-driven molecular gripping

Jovana V. Milić, Thomas Schneeberger, Michal Zalibera, François Diederich, Corinne Boudon, Laurent Ruhlmann

Spectro-Electrochemical Toolbox for Monitoring and Controlling Quinone-Mediated Redox-Driven Molecular Gripping

Jovana V. Milić [a,b,#], Thomas Schneeberger [a,#], Michal Zalibera [c], François Diederich [a,*], Corinne Boudon [d], and Laurent Ruhlmann [d,*]

[a] *Laboratory of Organic Chemistry, ETH Zurich, HCI, Vladimir-Prelog-Weg 3, 8093 Zurich, Switzerland*
[b] *Laboratory of Photonics and Interfaces, EPFL, Station 6, 1015 Lausanne, Switzerland*
[c] *Institute of Physical Chemistry and Chemical Physics, Slovak University of Technology, Radlinského 9, 81237 Bratislava, Slovakia*
[d] *Université de Strasbourg, Laboratoire d'Electrochimie et de Chimie Physique du Corps Solide, Institut de Chimie de Strasbourg, UMR 7177, 4 rue Blaise Pascal, CS 90032, 67081 Strasbourg, France*

# Authors contributed equally.

Abstract: The control of molecular systems by electrical charge or light is a prerequisite for their application in nanoelectronics. Such potential has been uniquely exploited in quinone-based resorcin[4]arene cavitands that can act as molecular grippers, reversibly expanding and contracting in response to electrical or electromagnetic stimuli. The development of such redox- and photoredox-driven gripper systems required employing a set of electrochemical, spectroscopic, and spectroelectrochemical techniques that have been applied to control and monitor the redox state and the geometry of grippers. Here, we provide a systematic overview of this spectro-electrochemical toolbox in the context of the quinone redox chemistry and molecular gripping, from cyclic and rotating disc voltammetry, through square-wave voltammetry and UV-Vis-NIR spectroelectrochemistry, to NMR, EPR, and ENDOR spectroscopy. The understanding of the molecular gripping process revealed through the lens of these techniques paves the way for more advanced molecular design and sets the basis for extending the utility of molecular grippers in the future.

Keywords: molecular grippers, supramolecular chemistry, spectroelectrochemistry, electroswitch, photoredox-switch

1 Introduction

Since their inception by Cram and co-workers in 1980s [1], resorcin[4]arene cavitands emerged as versatile platforms for host-guest complexation [2-4] and molecular sensing [5-8]. This unique behavior is based on their ability to switch between two conformations, an open (kite) and a closed (vase), which can reversibly encapsulate smaller molecules (Fig. 1a) and consequently act as molecular grippers [9-12]. The conformational switch can be controlled by a variety of stimuli (Fig. 1b), such as changes in temperature and pH [13], metal ions [14], redox processes [4,10-12,15,16], and light [17,18]. Introducing physical stimuli to control molecular gripping, such as electrical charge or light, is of particular importance to enable future applications in molecular electronics. This required an exploration of a variety of redox-active moieties, such as tetrathiafulvenes [19,20], ferrocenes [21], and quinones [15,22-24]. Inspired by their biological role in natural photosynthesis as redox acceptors [25-29], quinones (**Q**) have emerged as the suitable functionality in molecular grippers. This choice is particularly the result of the accessibility of multiple redox states through photo-redox processes, accompanied by long lifetimes of the reduced states (i.e. semiquinone radical anion ($\mathbf{SQ}^{\bullet-}$) and quinone dianion ($\mathbf{Q}^{2-}$) and their protonated analogues; (Scheme 1), as well as by the capacity of quinones to change their affinity for hydrogen bonding as a function of the redox state [11,12,30]. Progress in the research on quinone-based molecular grippers greatly benefited from the control and monitoring of the redox switch, which acts as a trigger for the conformational change, by using spectro-electrochemical tools.

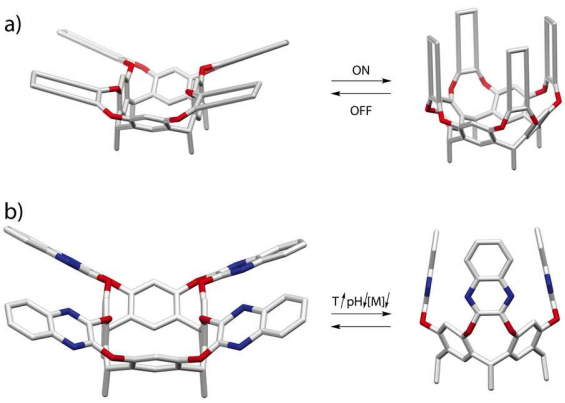

Fig. 1. (a) Schematic of molecular grippers that switch between two conformations, the open (kite, OFF) and the closed (vase, ON). (b) Model structure of the tetraquinoxaline resorcin[4]arene cavitand developed by Cram and co-workers responsive to temperature (T), pH variations, and different metal ion concentrations (M) by reversibly changing the conformation between the kite (left) and the vase (right) [1]. Hydrogen atoms are omitted, and hexyl chains in the lower rim are substituted for methyl groups for simplicity.

Some of the electrochemical methodologies established in the early work on redox-active macrocyclic supramolecular systems, such as calixquinones, have been proven particularly valuable in establishing a suitable approach.

For instance, Echegoyen and co-workers explored the multiple redox states of calix[4]quinones by using cyclic and rotating disc voltammetry, illustrating the possibility to control their properties in response to the electric charge [22-24]. Whereas the flexibility of calixquinones prevented their utility in bistable gripper-like switching, the corresponding electrochemical analytical approach was directly applicable to quinone-based resorcin[4]arenes, which were proven ideal platforms for developing molecular gripper analogues [4,10-12,15,16,31].

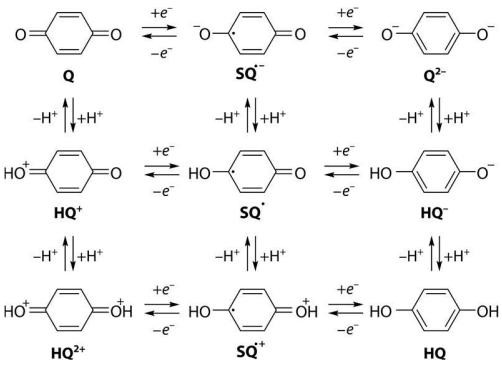

Scheme 1. Redox equilibrium between quinone (**Q**), semiquinone (**SQ**), quinone dianion (**Q**$^{2-}$), as well as their protonated intermediates.

Herein, we provide a systematic overview of the electrochemistry of quinones as well as the analytical toolbox for the development of photoredox-switchable molecular grippers, which involves techniques such as cyclic (CV), rotating disc (RDV), and square-wave voltammetry (SWV), UV-Vis-NIR spectroelectrochemistry (SEC), NMR, EPR, and ^{1}H Electron Nuclear Double Resonance (ENDOR) spectroscopy. The analysis is complemented by DFT calculations and the studies of model systems, which provides crucial insight into the underlying redox, conformational, and gripping processes.

2 Experimental Section

The experimental details are based on previously reported procedures [9-12,30-37].

2.1. Cyclic, Rotating Disc, and Squarewave Voltammetry

The CV and RDV experiments were carried out in a solution of CH_2Cl_2 at ambient temperature containing 0.1 M *n*-Bu_4NPF_6 in a classical three-electrode cell. The cell was equipped with a glassy carbon (GC) disc or Pt disc working electrode (WE), the Pt wire counter electrode (CE), and the Pt wire pseudo-reference electrode (RE) and connected to a potentiostat. The voltammetric scans were carried out at rates of 100 mVs^{-1}. SWVs were recorded with 25 mV pulse amplitude, 30 Hz pulse frequency, and 5 mV step increments.

2.2. UV-Vis-NIR Spectroelectrochemistry

In situ UV-Vis-NIR SEC experiments were performed with solutions of degassed CH_2Cl_2 or THF (1–2 mM) and 0.2 M *n*-Bu_4NBF_4 as the supporting electrolyte. A three-electrode arrangement with Pt mesh as WE, glassy carbon CE, and AgCl/Ag wire as pseudo-reference electrode was used in a thin layer optical cell with KBr windows.

2.3. EPR and ENDOR Spectroscopy

X-band (≈ 9.5 GHz) CW EPR measurements were performed at ambient temperature on a Bruker Elexsys E500 spectrometer with 2 mW applied microwave power and 0.01 mT field modulation. Q-band (≈ 34 GHz) pulse EPR and ENDOR was performed at 80 K using a Bruker ELEXSYS E580 Q-band pulse EPR spectrometer equipped with a home-build TE011 microwave cavity [32] and an Oxford-CF935 liquid helium cryostat. Electron spin echo (ESE)-detected field-swept spectra were acquired with the two-pulse Hahn-echo sequence t_p–τ–2t_p–τ–echo using t_p = 20 ns and τ = 358 ns [33]. ^{1}H ENDOR spectra were recorded using the Davies type t_{inv}–t_{RF}–T–t_p–τ–2t_p–τ–echo sequence [34] with t_{inv} = 200 ns, t_{RF} = 20 µs, t_p = 40 ns, T = 4 µs, τ = 480 ns. W-band (≈ 94 GHz) pulse EPR and ENDOR experiments were performed at 80 K with a modified Bruker Elexsys E680 spectrometer equipped with a home-built ENDOR cavity optimized for maximum radio-frequency (RF) performance around the proton Larmor frequency of ≈ 140 MHz [35]. Electron spin echo (ESE)-detected field-swept spectra were acquired by use of the two-pulse Hahn-echo sequence [33] t_p–τ–2t_p–τ–echo using t_p = 32 ns and τ = 316 ns. ^{1}H ENDOR spectra were recorded using the Davies type t_{inv}–t_{RF}–T–t_p–τ–2t_p–τ–echo sequence [34] with t_{inv} = 200 ns, t_{RF} = 20 µs, t_p = 32 ns, T = 5 µs, τ = 500 ns. Spectral analysis and EPR simulations were performed with the EasySpin toolbox [36]. The **SQ**$^{\bullet-}$ samples of model compounds were produced by the reduction of ~0.5 mM of the parent compounds with an excess of cobaltocene ($CoCp_2$) in degassed (three free-pump-thaw cycles, 0.01 mbar) CH_2Cl_2, CD_2Cl_2, or CD_2Cl_2/CD_3CN (5:1 v/v) directly in the EPR tubes [11]. The grippers were reduced by an excess of cobaltocene to obtain the bis-**SQ**$^{\bullet-}$ radical dianions and in less than 1:1 stochiometric ratio to get the single electron reduced **SQ**$^{\bullet-}$ radical monoanion. Deuterated solvents were used for preparation of samples for ^{1}H ENDOR spectroscopy, in order to avoid the signals due to the dipolar hyperfine interaction of the **SQ**$^{\bullet-}$ with the solvent. For ambient temperature experiments, the tubes were sealed under N_2 directly after the reduction and immediately transferred into the cavity of the EPR spectrometer. For low temperature measurements, the tubes were flash frozen in N_2 (l) and transferred to the cryostat of the spectrometer pre-cooled to 80 K [11,37].

2.4. NMR Spectroscopy

^{1}H NMR spectra were recorded on a Varian Mercury operating at 300 MHz or a Gemini operating at 400 MHz at 298 K unless otherwise specified. ^{13}C NMR spectra were recorded on a Bruker DRX 400 operating at 100 MHz. Chemical shifts δ (ppm) were referenced to the internal solvent signals.

3 Results and Discussion

3.1 Electrochemistry of Quinones

3.1.1. Biological Roles of Quinones

Quinones can undergo reversible reduction (electron transfer) combined with acid-base (proton transfer) reactions. Such redox process can be represented by a typical square scheme (Scheme 1) [23,38]. Quinone reduction reactions readily occur in proteins, such as the cytochrome bc_1 oxido-reductase, the NADH-quinone reductase, and succinate-quinone reductase in mitochondria or oxygenic bacteria [38]. Furthermore, other quinones, such as ubiquinones, are important functional units in numerous biological systems and act as lipid-soluble electron- and proton-carriers in photosynthetic electron flow systems, as well as in the membranes of mitochondria, chloroplasts, and bacterial cells [23,39-71]. Other types of quinones are present in anthracycline drugs and a class of anthraquinones can be used for anticancer treatments in numerous forms of human cancer, such as acute leukemia and malignant lymphomas [39-41,44,48,55-57,60,62,66-68,70-71]. Anthracyclines are also active in solid tumors, particularly in case of breast cancer, where it has been noticed that their biological activities are correlated with their redox behavior [39,42,46,59,61,65,69]. In the photosynthetic reaction centers, quinones play a key role in the transformations of the primary Q_A and the secondary Q_B site [63-64,72-75]. The quinone redox transformation is strongly affected by the environmental factors, such as aqueous or non-aqueous media, pH value, and presence of noncovalent interactions [23].

3.1.2. Electrochemical Reduction in Aqueous Media

In aqueous media, the quinone-hydroquinone couple (**Q**/**HQ**; Scheme 1) provides a classical example of a single step $2e^-$ redox couple in which potentials vary with pH according to the Nernst equation [62]. This redox behavior can be summarized using Pourbaix (E-pH) diagrams, which present regions of existence of various redox and protonated species as a function of their respective pK_a values [76-78]. In buffered aqueous media, anthraquinones and other *para*-quinones show a single reversible reduction wave by cyclic voltammetry. In acidic solution, however, the reduction involves a single step $2e^-/2H^+$ process to form the **HQ** [38,79-82], while in alkaline solutions this process involves a $2e^-$ reduction to the quinone dianion ($\mathbf{Q}^{2-}$) without protonation. On the contrary, in neutral solutions, the reduction can either involve one proton and $2e^-$ ($\mathbf{HQ}^-$ formation) or only $2e^-$ without protonation ($\mathbf{Q}^{2-}$ formation; Scheme 1), which depends on the medium [23,83–85]. Only few studies on the redox behavior of quinones in unbuffered aqueous media have been reported [76,86-95]. Under these conditions, the proton concentration dictates the outcome of the redox process. Depending upon the pK_a of the species, the intermediates $\mathbf{SQ}^{\bullet-}$, **HQ**, $\mathbf{HQ}^-$, or $\mathbf{Q}^{2-}$ can be stabilized by hydrogen bonding. In general, the environmental factors dictate the outcome of the **Q** redox interconversion process.

3.1.3. Electrochemical Reduction in Non-Aqueous Media

In non-aqueous media, the reductions of quinones occurs via two successive $1e^-$ transfer steps generating two distinct cathodic waves. The first step is fully reversible and corresponds to the formation of the $\mathbf{SQ}^{\bullet-}$, while the second step is often quasi-reversible and results in the $\mathbf{Q}^{2-}$ formation [96-106]. Polarity of the solvent, type of conducting electrolyte, protonation-deprotonation equilibria, ion-pair formation, as well as intra- and intermolecular hydrogen bonding, play a significant role in the two successive reduction potentials [23]. Addition of hydrogen bonding agents can stabilize the $\mathbf{SQ}^{\bullet-}$ as well as the $\mathbf{Q}^{2-}$ *via* intermolecular hydrogen bonds. Subsequently, the two successive reduction potentials shift towards more positive values in presence of such hydrogen bonding agents [96,107-109]. For instance, gradual addition of water to DMF or DMSO solutions of quinones leads to positive shifts of the second reduction potential until the second wave fuses with the first reduction. This behavior can be explained by the stabilization of $\mathbf{Q}^{2-}$ through hydrogen bonding [107,110-111].

In addition to hydrogen bonding and protonation, other processes take place in the quinone redox equilibria, including disproportionation, [76] comproportionation, [23,38,97,98,111-115] and dimerization,[106] which can affect the general electrochemical reactions [23]. Semiquinone radical anions ($\mathbf{SQ}^{\bullet-}$) can undergo disproportionation in solution [76]. These redox interconversions must be carefully taken into consideration when analyzing more complex quinone-based molecular architectures, such as the calixquinones.

3.1.4. Electrochemistry of Calix[4]arenequinones

Calixarenes have received considerable attention because of their ability to bind ions or molecules, acting as receptors used for host-guest complexation [116]. Electroactive calixarenes comprising a redox-active group, such as a quinone, are thereby even more attractive due to the possibility to control their properties electrochemically [116-117]. A series of four *para*-benzoquinone-containing calix[4]arenes have been synthetized. Mono-, di-, tri-, and tetra-quinone-based calix[4]arenes exhibit successive one electron transfers in dry CH_3CN corresponding to each of the quinone subunits (Scheme 2, top). For each *para*-benzoquinone unit, reversible two $1e^-$ reductions were detected giving $\mathbf{SQ}^{\bullet-}$ and $\mathbf{Q}^{2-}$ in dry acetonitrile as a solvent [24,118]. The redox behavior was shown to be analogous to that of *para*-benzoquinone [76].

Calix[4]tetraquinone consists of four para-benzoquinone units connected by $-CH_2-$ groups (Scheme 2, top). Each *para*-benzoquinone unit undergoes reversible two single-electron reductions to form $\mathbf{SQ}^{\bullet-}$ and $\mathbf{Q}^{2-}$ in dry CH_3CN and the four para-benzoquinone units are reduced successively [24]. The first two *para*-benzoquinone units are reduced at less negative potentials while the reductions of the two other units are detected at more negative potentials (Table 1). The difference in redox potentials between the second and third step were considerably larger than those between the first and second step, as well as the third and

the fourth step. It suggests that the first two electron processes take place at the opposing *para*-benzoquinone subunits (Table 1). The third electron transfer, however, occurs at the second *para*-benzoquinone unit, which is located between the two *para*-benzoquinone radical anions, resulting in a large resistance to the incoming electron. This explains the potential differences between the first and the second wave, as well as the third and the fourth wave.

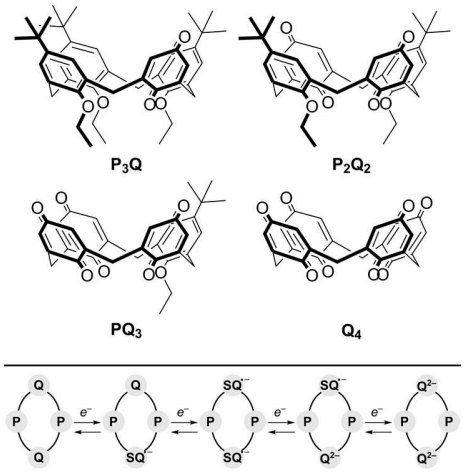

Scheme 2. Top: Examples of calix[4]arenequinones studied by Echegoyen et al. that provided the basis for the electrochemical analysis of quinone-equipped resorcin[4]arenes [22-24]. Bottom: Schematic representation of the redox interconversion of a calix[4]arenediquinone. P = phenolether, Q = para-benzoquinone.

Table 1. $E_{1/2}$ (V) for calix[4]arenequinones in CH_3CN *vs.* AgCl/Ag.[a,b]

	$E_{1/2}{}^1$	$E_{1/2}{}^2$	$E_{1/2}{}^3$	$E_{1/2}{}^4$	$E_{1/2}{}^5$	$E_{1/2}{}^6$
P_3Q	–0.82	–1.45	–	–	–	–
P_2Q_2	–0.70	–0.84	–1.22	–1.43	–	–
PQ_3	–0.51	–0.75	–0.98[c]	(–1.35)[d]	–1.48	–
Q_4	–0.43	–0.55	(–0.93)[d]	(–1.07)[d]	–1.12	–1.24

[a] Data is based on ref. [22-24]. [b]All potentials *vs.* AgCl/Ag reference, all scan rates at 100 mVs^{-1} unless otherwise noted. [c] Potential obtained by differential pulse voltammetry (20 mVs^{-1} scan rate). [d] Values in parentheses are cathodic peak potentials not half-wave potentials. P = phenolether, Q = para-benzoquinone.

In the case of calix[4]arenediquinone, four successive one-electron transfers to the two *para*-benzoquinone units are observed (Scheme 2, bottom). These can be assigned to the electron transfers into each of the available quinone units, giving bis-semiquinone radical anion (bis-**$SQ^{\bullet-}$**). The two subsequent reductions correspond to the reduction to the corresponding bis-dianion (bis-**Q^{2-}**). In this case, upon the addition of metal ions, new set of reduction peaks were observed at more positive potentials in comparison to the initial quinone waves. This shows a stabilization of the reduced form, radical anion or dianion, in the presence of metal ions [119-122].

Based on their electrochemical properties and sensing ability, the electrochemical analysis of calix[4]arenediquinones was closely applicable to quinone-based resorcin[4]arenes, as platforms for developing molecular grippers detailed in the following sections.

3.2 From Redox-Active Cavitands to Photo-Redox Switchable Molecular Grippers

The need for systems that are responsive to electric charge stimulated the development of the first quinone-based redox-active resorcin[4]arene cavitand **1** by Diederich and co-workers (Fig. 2a) [15]. The cavitand in the oxidized quinone (**Q**) state could be chemically reduced by using H_2/Pd in protic solvents (CH_3Cl/H_2O) to form the hydroquinone (**HQ**) state. As changes in the redox state did not result in the conformational changes required for redox-switchable analogues, cavitand **1** was modified by introducing hydrogen bond acceptor groups (Fig. 2b). This approach was particularly effective in case of the carboxamide groups to form **2**. As a result, reduction to the **HQ** state not only altered the electronic properties, but it was accompanied by a conformational change to the closed form stabilized by hydrogen bonding between the hydroxyl groups of the hydroquinone and the carboxamide. This reaction was, however, strongly dependent on the proton source and limited by poor reversibility in the **HQ** state. As a result, the control of this redox process was not possible electrochemically [4].

To alter the properties of this system electrochemically in aprotic environments, it was essential to focus on the semiquinone radical anion (**SQ**) state, which could be accessed both electrochemically and photochemically (Fig. 2c) [23,123]. Furthermore, to ensure that the conformational change follows the redox switch, this system was equipped with hydrogen bond donating groups, such as pyrrole (Fig. 2d), to drive the conformational switch based on hydrogen bond strengthening upon reduction to the **SQ** state. The formation of the desired **SQ** state was performed (i) electrochemically, via cyclic voltammetry (CV), (ii) chemically, through reduction of the **Q** with $CoCp_2$, and (iii) photochemically, by using $[Ru(bpy)_3]^{2+}$ as a photoreductant in the presence of Et_3N as sacrificial electron donor in CH_2Cl_2 upon photoexcitation [11]. The photoreduction process was observed by identifying the spectroscopic signature via UV-Vis-NIR spectroelectrochemistry and EPR spectroscopy [11,124,125], as well as transient absorption spectroscopy [125]. Moreover, the hydrogen bonding that facilitated the conformational change, as well as alteration of the electronic, magnetic, and photophysical properties, was probed by CV, SWV, and ENDOR spectroscopy. Finally, the gripping properties were assessed by NMR, CV, and SWV, as addressed in detail within the following sections.

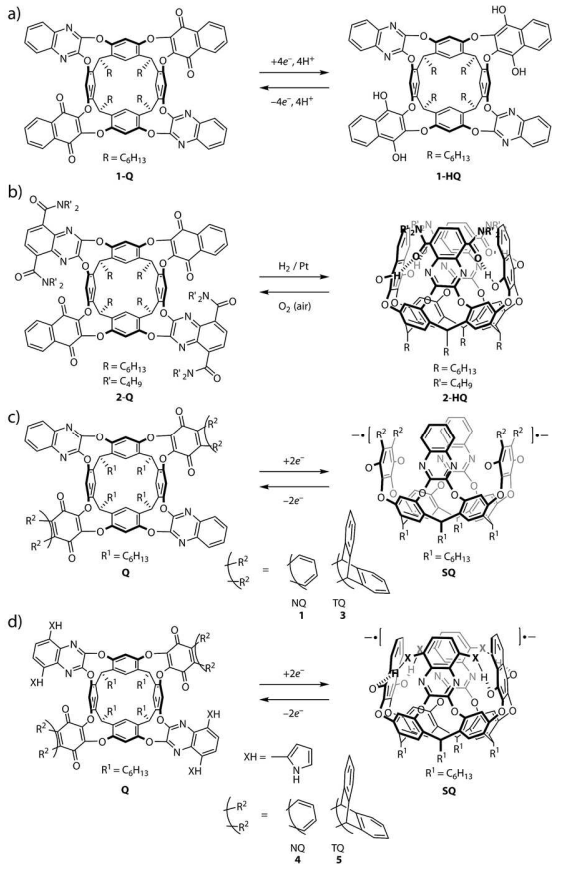

Fig. 2. Structural representation of quinone-based resorcin[4]arene cavitands developed by Diederich and co-workers [15]. (a) Redox-active (**1**) and (b) redox-switchable (**2**) cavitands and their **Q**-**HQ** equilibrium [10,16]. (c–d) Electro- and photoredox-switchable cavitands (**1**,**3**) based on (c) the **Q**-**SQ** equilibrium [11] and (d) **Q**-**SQ** equilibrium driven by hydrogen bonding (**4**–**5**) [12]. When referring to the cavitand redox states, **Q** refers to the one containing two quinone walls (2**Q**), **HQ** two hydroquinone walls (2**HQ**), and the **SQ** state refers to the bis(radical anion) (2**SQ**$^{\bullet-}$), unless otherwise specified.

3.2.1. Electroswitching of Quinone-Based Cavitands: Cyclic/Rotating Disc Voltammetry and Model System Analysis

The simultaneous electrochemical generation and monitoring of the **SQ** state formation electrochemically can be achieved by using CV and RDV. The reduction conditions were established via investigation of model compounds **6** and **7** (Fig. 3a–b), which represent single cavitand walls. Their analysis led to the identification of the spectroscopic signatures of the target **SQ** intermediates that could then be used to understand the behavior of the corresponding cavitand systems [11].

Cyclic voltammograms of **6** and **7** show two successive reduction steps at –1.01 V and –1.58 V for model **6**, and –0.84 V and –1.44 V for model **7** (*versus* Fc$^+$/Fc as an internal standard) on glassy carbon (GC) electrodes in *n*-Bu_4NPF_6 solutions in CH_2Cl_2 at ambient temperature (Fig. 3c–d). The **SQ** generation took place in the first reversible reduction step, and the second quasi-irreversible reduction wave resulted in the formation of the quinone-dianion **Q**$^{2-}$ (Fig. 3c–d). The **SQ** formation was facilitated for the triptycenequinone-based model **7** compared to napthoquinone-based **6**, as reflected in the anodically shifted reduction potential. Moreover, each step corresponded to a 1*e*$^-$ reduction, as shown by the rotating disc voltammetry (RDV; Fig. 3e–f) [11]. Having identified the strategies to generate and analyze **SQ** states electrochemically on the basis of the model systems **6** and **7**, the methodology could be used to investigate the corresponding cavitands **1** and **3** (Fig. 2a,2c and Fig. 4).

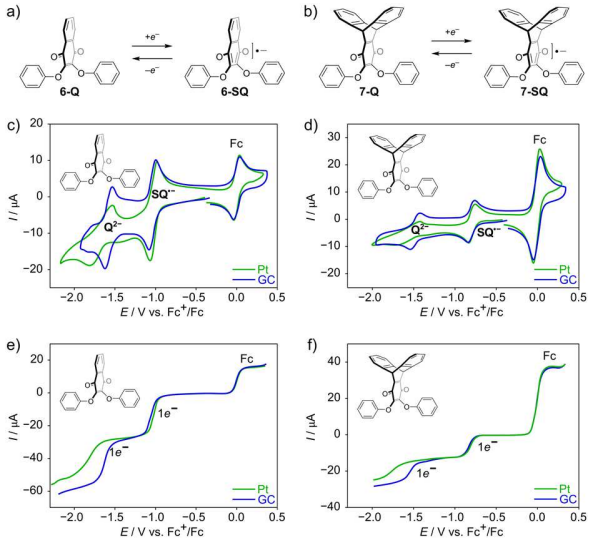

Fig. 3. Top: Formation of the **SQ** states of models (a) **6** and (b) **7** by 1*e*$^-$ reduction of the corresponding **Q** states. Bottom: CV of (c) **6** and (d) **7** and RDV of (e) **6** and (f) **7** in 0.1 M *n*-Bu_4NPF_6/CH_2Cl_2 at scan rates of 0.1 Vs^{-1} on GC electrode (blue) and Pt electrode (green). Ferrocene (Fc$^+$/Fc) is used as internal standard. GC = glassy carbon; Fc = ferrocene.

The CV of **1** and **3** in CH_2Cl_2 revealed a three-step reduction, with reduction potentials of –1.10 V, –1.62 V, and –2.19 V in case of **1** (Fig. 4a), and –0.88 V, –1.55 V, and –2.22 V (*vs.* Fc$^+$/Fc as an internal reference) for **3** (Fig. 4b), respectively. The RDV showed that each reduction step of both **1** and **3** occurs as a 2*e*$^-$ process, in accordance with a concerted reduction of the two redox-active **Q** walls. Importantly, the first reduction step ascribed to the formation of the **SQ** state was found to be fully reversible, particularly on GC electrodes, suggesting the suitability of this redox process for molecular switching. The two successive quasi-reversible reductions correspond to the formation of the quinone dianion **Q**$^{2-}$ and the reduction of the quinoxaline (Qx) core that were not directly employed in the molecular switch.

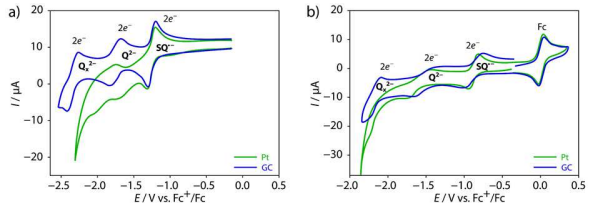

Fig. 4. Cyclic voltammetry of (a) **1** and (b) **3** in 0.1 M *n*-Bu_4NPF_6/CH_2Cl_2 at scan rates of 0.1 Vs^{-1} on glassy carbon GC electrodes (blue) and Pt electrode (green). Fc is used as internal standard.

3.2.2. Semiquinone-Based Cavitands: UV-Vis-NIR Spectroelectrochemistry and EPR Spectroscopy

The spectroscopic identification of the **SQ** state can be based on the unique SOMO-LUMO transitions that result in the absorption in the visible range [11,126,127]. This absorption could be monitored *in situ* upon electrochemical reduction by using UV-Vis-NIR spectroelectrochemistry [124]. Such an approach was defined based on models **6** and **7** that represent single cavitand walls and extended to the corresponding cavitands as prospective molecular grippers [11,37].

UV-Vis-NIR spectra of **6** and **7** upon electrochemical reduction in the domain of the first reduction wave show absorption in the area between 450–550 nm, which indicates the **SQ** formation (Fig. 5a–b). The reversibility of this redox exchange between the **Q** and the **SQ** states can be examined by performing the UV-Vis-NIR spectroelectrochemistry measurements over several reduction-oxidation cycles and monitoring the changes of the absorbance in the visible region. This approach revealed the high reversibility of the redox interconversion with low fatigue resistance for both models **6** and **7** (Fig. 5c–d). With the reversible formation of the **SQ** of the model systems, the spectroscopic indicators were assessed in the prospective grippers **1** and **3**.

Similar to the observations in the models, UV-Vis-NIR spectroelectrochemical experiments showed absorption in the 400–500 nm region, characteristic for the **SQ** states, upon reduction of **1** and **3** (Fig. 6a). This signature was present for different cavitands after $2e^-$ reduction, which enabled it to serve as a unique fingerprint for the corresponding **SQ** formation [127-130]. Moreover, the evolution of the absorption in the UV-Vis-NIR spectra over recurrent reduction-oxidation cycles also demonstrated high reversibility of the **SQ**–**Q** transformation (Fig. 6b), documenting the molecular switching as a basis for molecular grippers.

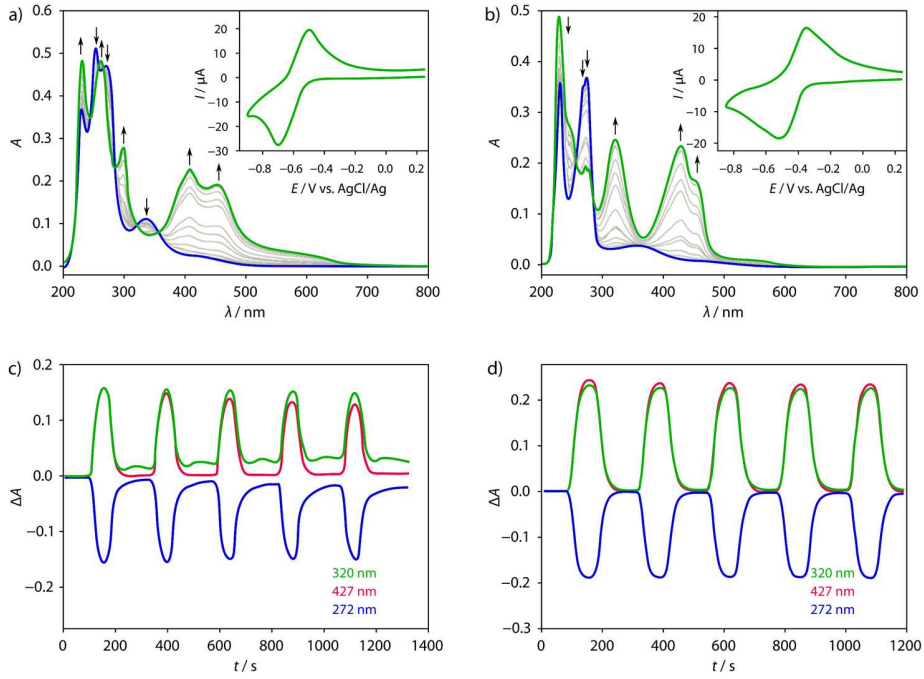

Fig. 5. UV-Vis-NIR spectroelectrochemistry of models (a) **6** and (b) **7** at ambient temperature upon electrochemical reduction in 0.1 M n-Bu_4NPF_6 in CH_2Cl_2 in the potential region of the first reduction step at scan rate of 10 mVs^{-1}. Inset shows the CV at scan rate of 20 mVs^{-1}. Evolution of the UV-Vis-NIR spectra recorded during reduction in CH_2Cl_2 of models (c) **6** and (d) **7** over several redox-switching cycles demonstrate the reversibility of the redox interconversion with color-coded spectral ranges. In a) and b) blue color corresponds to the spectra of initial **Q** form while green color is for the **SQ** form (100% of conversion).

The reversible $2e^-$ reduction of the cavitand might result in the formation of two different **SQ** species; the first being a diamagnetic **SQ**, with antiferromagnetically coupled spins, adopting a singlet spin state ***S*** ($S = 0$). The other species features ferromagnetic spin coupling and results in a paramagnetic **SQ** bis(radical anion) in the triplet spin state ***T*** ($S = 1$) [129,131]. DFT calculations at the B3LYP/6-31G(d) level of theory indicate that the triplet spin states are favored for **SQ** bis(radical anion) of **1** and **3** [11,37]. Their paramagnetic nature allowed a detail characterization by EPR spectroscopy [132-134]. The echo-detected (ED) EPR spectra of reduced cavitands **1** and **3** show g tensors that correspond to those typically observed for **SQ** bis(radical anion) (Table 2, Fig. 7a–d) [30,126-129,134]. However, the ED EPR spectra featured contributions from two paramagnetic species. The main species corresponded to the **SQ** bis(radical anion) of **1** and **3** in the triplet spin state ***T*** ($S = 1$), since it displayed a resolved fine structure resulting from the dipole-dipole interaction of the two unpaired electron spins in $\mathbf{1}^{2-}$ (blue arrow, Fig. 7c) and $\mathbf{3}^{2-}$ (red arrow, Fig. 7a). On the other hand, the minor paramagnetic species (purple arrow in Fig. 7d and green line in

Fig. 7b) resulted from the formation of the radical monoanion in the doublet spin state ***D*** (S = ½). Such state typically forms in solutions of **SQ** bis(radical anion) by disproportionation reactions [23,78,135]. The ED EPR spectra can be a simulated (red line in Fig. 7c and 7d) using the Spin Hamiltonian parameters summarized in Table 2.

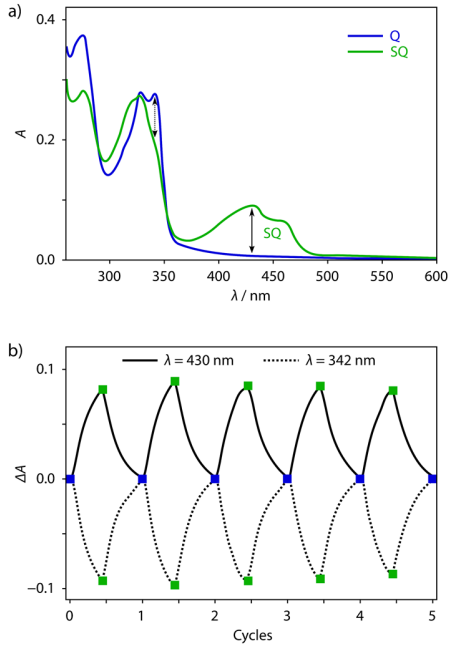

Fig. 6. (a) UV-Vis-NIR spectra of the **Q** and the **SQ** states of **3** (1 mM) in n-Bu_4NBF_4/CH_2Cl_2 (0.2 M) recorded during the first reduction wave. (b) Evolution of the absorption maxima in the spectrum presented in a) for several redox cycles. Adapted with permission from ref. [11]. Copyright 2016 American Chemical Society.

Table 2. EPR data, Spin Hamiltonian of triplet **SQ** of **1**–**3**.

	g-tensor[a]	ZFS	Distance
SQ	g_x, g_y, g_z	D, E / MHz[b]	r / Å[c]
1	2.0070, 2.0052, 2.0025	77.8, 3.1	10.0
3	2.0074, 2.0056, 2.0026	78.1, 3.1	10.0

[a]±0.0001; [b]±4 MHz; [c]±0.5 Å; ZFS = zero field splitting.

The assignments of both paramagnetic species identified by ED EPR spectroscopy can be confirmed by electron spin echo nutation (ESN) experiments [132-134]. In this experiment, a preparation microwave pulse of variable duration is inserted in the pulse sequence before the Hahn ED block, which leads to an oscillation (i.e. nutation) of the EPR signal as a function of the preparation pulse duration (Fig. 7a,c). The oscillation frequency (i.e. nutation frequency, ν_{nut}) is related to the microwave field strength (in angular frequency units, ω_1). The dependence is expressed through the proportionality factor α that includes the spin quantum numbers (S, m_s) of the state involved in the excited EPR transition according to the equation (1). The α factor values in the S = ½ and S = 1 spin states are $\alpha = 1$ and $\alpha = \sqrt{2}$, respectively (Table 3).

$$2\pi\nu_{nut} = \alpha \cdot \omega_1 , \qquad \alpha = \sqrt{S(S+1) - m_s(m_s \pm 1)} \qquad (1)$$

Table 3. EPR transitions and factors α for the spin S.

S = ½		S = 1	
m_s transition	α	m_s transition	α
$\|-1/2\rangle \rightarrow \|1/2\rangle$	1	$\|-1\rangle \rightarrow \|0\rangle$	$\sqrt{2}$
		$\|0\rangle \rightarrow \|1\rangle$	$\sqrt{2}$

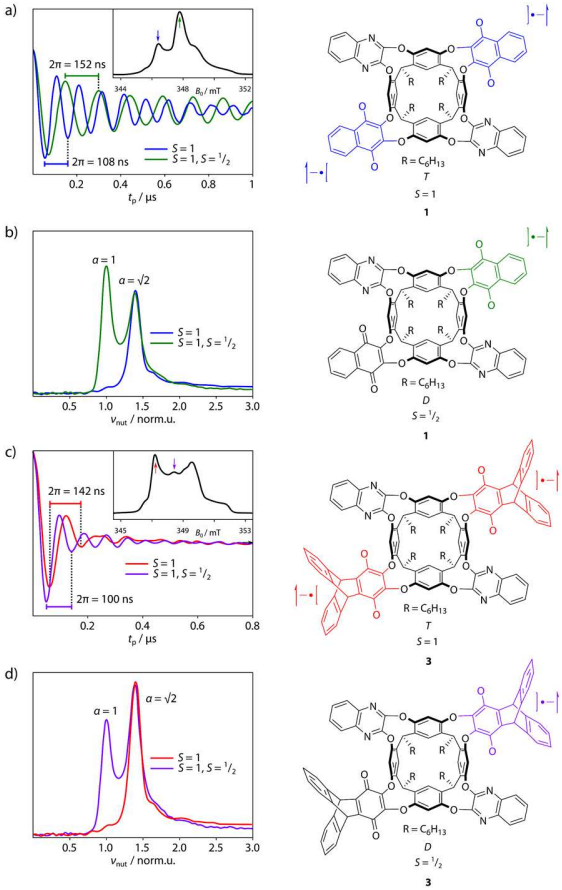

Fig. 7. ESN curves of the **SQ** states of (a) **1** and (c) **3** obtained at field positions marked by the arrows in the inset of the corresponding color of the curves. Insets present the ED EPR spectra of **SQ** states of **1** and **3** in CD_2Cl_2 at 80 K using the t_p–τ–2t_p–τ–echo sequence with t_p = 30 ns and τ = 150 ns. ESN spectra of the **SQ** states of (b) **1** and (d) **3** obtained at field positions marked by the arrows in the ED EPR spectra (inset of a) and c) curves) whose color corresponds to the spin nutation spectra. ESN = Electron spin nutation.

The ν_{nut} of the dominant signal is 1.41 ($\sqrt{2}$) times higher than that observed for the minor signal, which is expected for the triplet ***T*** (S = 1) and the doublet ***D*** (S = ½) species (Table 3, Fig. 7b,d). The ESN analysis thus confirms the spectral assignments of the triplet **SQ** dianion (S = 1, red for **3** and blue

for **1**) and a **SQ** monoanion ($S = ½$; purple for **3** and green for **1**) [23,78,135].

EPR experiments verified the formation of the paramagnetic **SQ** species in the triplet spin state upon two-electron reduction of the cavitands. The electronic properties of the prospective grippers have been further studied to understand the role of hydrogen bonding and control the conformational preferences after the redox interconversion [37].

3.2.3. Hydrogen-Bonded Semiquinone-Based Cavitands: Square-Wave Voltammetry and ENDOR Spectroscopy

The role of hydrogen bonding in the **SQ** state was extensively studied in the case of ubiquinones of the photosynthetic organisms and analogues [26,129,136-143]. These studies mainly employed CV and ^{1}H ENDOR spectroscopy. In order to categorize the effects of hydrogen bonding in the **SQ** state on its properties, we investigated model compounds **6** and **8**–**15** that mimic single gripper walls (Fig. 8). Moreover, we compared models comprising protected hydrogen bond donating groups (**8**, **10**, **12**, and **14**) to their unprotected analogues (**9**, **11**, **13**, and **15**). The effect of hydrogen bonding on the redox properties was investigated by CV and SWV, since stabilization of the **SQ** radical anions results in the shifts of the reduction potentials to more positive values [23,111,142,144-147].

Voltammograms revealed two key indicators of hydrogen bonding in the **SQ** state (Fig. 8b): (1) the shift of the first reduction potential to more positive values upon stabilization of the **SQ** [111]; and (2) the loss of reversibility of the second reduction wave, which likely occurred due to the protonation of the $\mathbf{Q}^{2-}$ in the presence of hydrogen bond donating groups [111,144]. The shifts were more pronounced for proximal groups (model **11**) than those that were distant for hydrogen bonding (model **9**). The loss of reversibility of the second reduction wave occurred in presence of both proximal and distant hydrogen bonding donating groups, even if not followed by potential shifts (e.g. model **9**; Fig. 8b). This observation allowed to exclude the influence of intermolecular hydrogen bonding on the shifts of the redox potential since the distant hydrogen bond donating groups did not induce shifts of the reduction potential of model **9**. Furthermore, this effect of hydrogen bonding on the redox properties depended on the bonding strength and were more pronounced for systems with stronger hydrogen bond donating groups (e.g. hydroxyl; Fig. 8b) closer to the carbonyl group in the **SQ** state, and less pronounced for moderate hydrogen bond donating groups (e.g. pyrrole or pyrazole in models **12**–**15**; Fig. 8c,d). Comparable effects could be observed by CV of **6** in the presence of excess pyrrole in solution, which suggested that HB of systems with moderate HBD groups also display all the HB indicators in higher concentrations (Fig. 8d), which was confirmed by similar effects of intramolecular hydrogen bonding of model systems **13** and **15** (Fig. 8c). Finally, with these hydrogen bonding indicators identified with the models, we have analyzed the voltammograms of pyrrole-containing **4**. It did display the shift of the first reduction potential to more positive values as compared to its *N*–*Boc* protected analogue **16** (Fig. 9), evidencing hydrogen bonding in the **SQ** state.

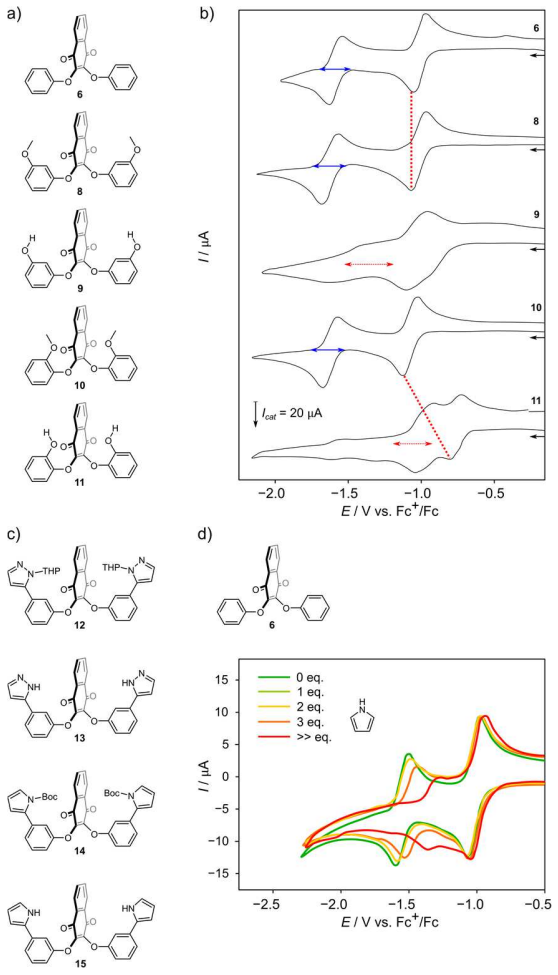

Fig. 8. (a) Models containing hydroxyl hydrogen bond donating groups (**9**, **11**) and the unsubstituted or protected analogues (**6**, **8**, **10**). (b) CV in CH_2Cl_2 at ambient temperature. Positive shifts of the first reduction potential (dashed red line) and the loss of reversibility of the second reduction waves (red arrows) compared to quasi-reversible reduction for protected hydrogen bond donating groups (blue arrows) indicate **SQ** stabilization. (c) Models **13** and **15** containing moderate hydrogen bond donating groups and their *N*-protected analogues **12** and **14**. (d) CV of **6** upon addition of increasing concentrations of pyrrole suggest intermolecular HB by positive shifts of the first reduction potential and loss of the reversibility of the second reduction wave. Adapted with permission from ref. [11]. Copyright 2016 American Chemical Society.

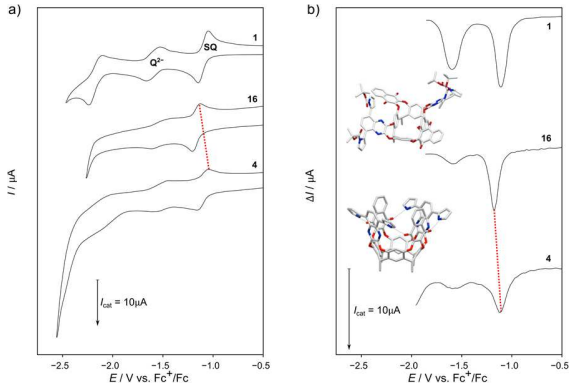

Fig. 9. (a) CV and (b) SWV of cavitands **4** and **16** and reference **1** in CH_2Cl_2 with 0.1 M n-Bu_4NBF_4 at a scan rate of 100 mVs^{-1} in the presence of ferrocene. Adapted with permission from ref. [12].

The interactions of the paramagnetic **SQ** species with the neighboring nuclei can be characterized by the hyperfine coupling (*hfc*) between the unpaired electrons and the corresponding hydrogen bonding proton (Fig. 10) [129,134,138,139,142]. This effect can be analyzed by ^{1}H ENDOR spectroscopy [148]. For instance, Davies ^{1}H ENDOR spectra of model **15** equipped with hydrogen bond donating groups show signals in the $|A|<4$ MHz range that correspond to the *hfc* of the backbone protons (Fig. 10a–d). The mono-reduced *N*-protected model **14** shows no contributions from the coupling with the neighboring hydrogen bond donating groups (Fig. 10b). On the contrary, the spectra of reduced **15** displays additional *hfc* with $|A|>4$ MHz. This confirms stabilization by intramolecular hydrogen bonding in the **SQ** state (Fig. 10d). Moreover, the ENDOR spectra are orientation-selective, which provides information about the geometry of the interacting species. In the case of model **15,** it reveals that the geometry of the hydrogen bonding is distorted when compared to the intermolecular HB complexes of **SQ** with protic solvents [12]. This is in accordance with the DFT calculated model (shown in Fig. 10c) and similar to the ubiquinone in the bacterial RC [26,129,136-143]. In addition to the model compounds, such intramolecular stabilization was also evidenced by ^{1}H ENDOR spectroscopy of single electron reduced cavitand **4** that shows additional *hfc* with the hydrogen bond donating group, in this case pyrrole, confirming the hydrogen bonding in the **SQ** state (Fig. 10e–f).

These interactions in the **SQ** state are directly affecting the conformational preferences, which can be further assessed by a combined spectro-electrochemical approach relying on UV-Vis-NIR spectroelectrochemistry, NMR, and EPR spectroscopy.

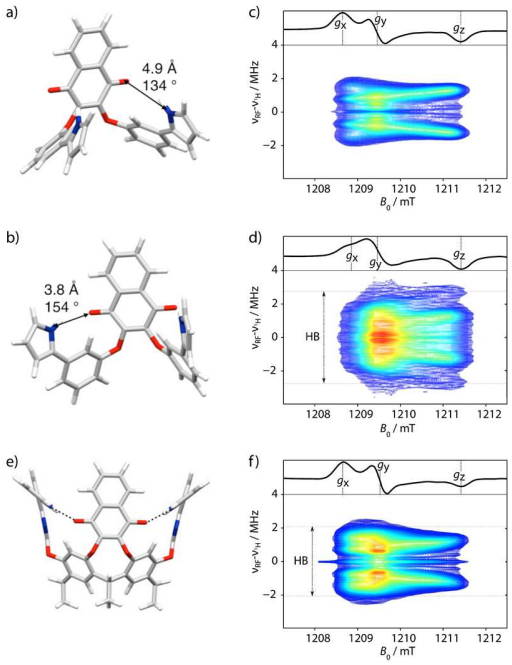

Fig. 10. Structural representations of model **15** in the (a) **Q** and (b) **SQ** state [37]. ^{1}H Davies Q-band (34 GHz) ENDOR spectra of models (c) **14** and (d) **15** as well as (f) gripper **4** in the **SQ** states (S = 1/2) generated by chemical reduction with $CoCp_2$ in CD_3CN under inert argon atmosphere at 80 K. Spectra were taken at magnetic field positions corresponding to g_x, g_y, g_z as indicated by the colored lines in the corresponding EPR spectrum shown in the top panel. Dotted arrows indicate the ENDOR signals due to *hfc* with the hydrogen(s) involved in the weak intramolecular hydrogen bonding. Adapted with permission from ref. [12].

3.2.4. Cavitand Geometry: From NMR Spectroscopy and Spectroelectrochemistry to EPR Spectroscopy

Conformational equilibrium between the open and closed forms of resorcin[4]arenes is mostly studied by ^{1}H NMR spectroscopy [15]. However, since unpaired electrons lead to broadening and disappearance of NMR signals [149-151], NMR spectroscopy cannot be used to characterize the geometry in the **SQ** states. An alternative technique that can provide information about the conformation is UV-Vis spectroscopy, relying on the Frontier molecular orbital changes for different conformations (Fig. 11) [13]. It has been shown that the quinoxaline cavitand conformation can be monitored by the changes in the 300–350 nm absorption domain (Fig. 11a). The origin of the absorption in this domain was verified by the analysis of model **17,** which corresponds to a single quinoxaline wall (Fig. 11b) [11]. We demonstrated that quinone-quinoxaline-based cavitands **1** and **3** in either the **Q** or **HQ** state exhibit similar UV-Vis spectral signatures in this absorption domain (Fig. 11a). To identify both conformations in the **Q** state by UV-Vis-NIR spectroscopy, we induced the changes in the conformational equilibrium by using solvent effects [4,11,15]. The stabilization of the open conformation is dominant in chlorinated solvents, such as CH_2Cl_2, whereas the

closed conformation is stabilized in other solvents, such as tetrahydrofuran (THF), at ambient temperature [4,15]. For the NMR-confirmed open conformation of **1** and **3** in their **O** state in CH_2Cl_2, we have identified two absorption maxima at 344 nm and 332 nm. On the other hand, the conformational change to the closed form correlates with a ca. 15 nm hypochromic and hypsochromic shift of these absorptions in THF (Fig. 11a). These effects are not evident for models that represent single gripper walls, such as **17**, since UV-Vis-NIR spectra in CH_2Cl_2 and THF are superimposable (Fig. 11b). The shifts of the absorption could thereby be related to the conformational change.

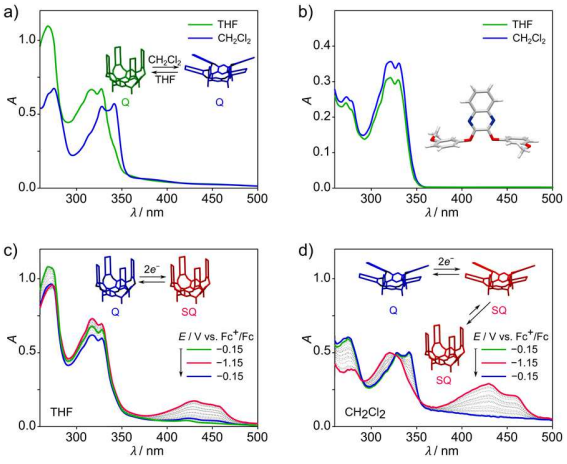

Fig. 11. (a) UV-Vis-NIR spectra of **3** in the **O** state in CH_2Cl_2 (open form) and THF (closed form) with a schematic of a conformational switch between the open (blue) and closed (green) forms in the **O** state. (b) UV-Vis-NIR spectra of model **17** in CH_2Cl_2 and THF and its crystal structure. (c) UV-Vis-NIR spectroelectrochemistry of **3** (1 mM) in *n*-Bu_4NBF_4/THF (0.2 M) with a schematic of a redox switch between the **SQ** (red) and the **O** (blue) state in the closed forms. (d) UV-Vis-NIR spectroelectrochemistry of **3** (1 mM) in *n*-Bu_4NBF_4/CH_2Cl_2 (0.2 M) with a schematic of a redox switch between the **O** (blue) in the open form and the **SQ** bis(radical anion) (red) state in the open and closed forms. The spectra correspond to the potentials indicated by colored lines in the inset. Adapted with permission from ref. [11]. Copyright 2016 American Chemical Society.

Having UV-Vis-NIR spectroelectrochemistry to monitor the gripper-like conformational change, the conformations of **1** and **3** were analyzed in the **SQ** state (Fig. 11c,d). The change of solvent or temperature did not affect the **SQ** absorption in the 400–500 nm range, however, the quinoxaline absorption at 300–350 nm suggested conformational changes upon reduction. The **SQ** states in THF directly corresponded to the closed form of the **O** state, with two absorption maxima at 329 nm and 320 nm (Fig. 11c). However, the UV-Vis-NIR spectrum in CH_2Cl_2 at ambient temperature displayed a ca. 10 nm hypo-hypsochromic shift of the signal that indicates opening upon reduction (Fig. 11db). This equilibrium shifts in CH_2Cl_2 are assumed to be the result of electrostatic interactions with the neighboring quinoxaline walls [4,10,16]. Similarly, for systems containing hydrogen bond donating groups (Fig. 12), hydrogen bonding should stabilize the closed conformation, which was analyzed in pyrrole-based cavitands (**4**–**5**).

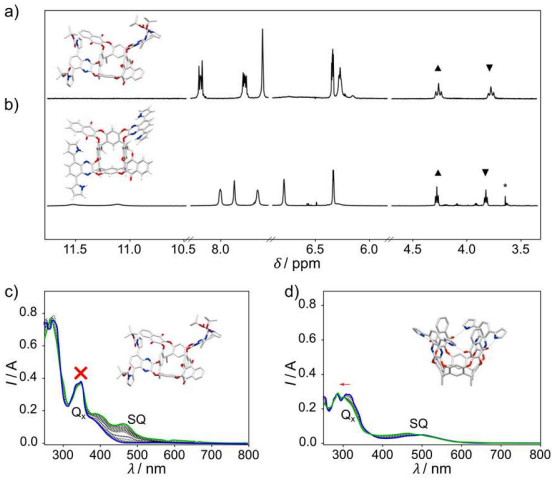

Fig. 12. Sections of ^{1}H NMR spectra of *Boc*-protected **16** (a) and pyrrole-based **4** (b) in the **O** state in $CDCl_3$ (400 MHz) at ambient temperature stabilized in the open conformation, as revealed by methine proton (▲▼) resonances in the 3.4–4.5 ppm domain. Sections comprising solvent peaks (7.25 ppm), hexyl chains (0–2.5 ppm), and no signals (8.5–10.5 ppm) were omitted for clarity. UV-Vis-NIR spectra of (c) *N-Boc* protected **16** and (d) its pyrrole-containing analogue **4** recorded upon electrochemical reduction at –1.1 V (vs. Fc^+/Fc) with schematic representations of grippers in the closed (top) and the open (bottom) form. Insets show structural representations of (a) **16** and (d) **4** in the oxidized **O** (open form, c and b) and the reduced **SQ** (closed form, d) state, respectively. Hexyl chains are replaced by methyl groups and hydrogen atoms are omitted for clarity. Adapted with permission from ref. [12].

^{1}H NMR spectra of pyrrole-containing **4**–**5** in $CDCl_3$ at ambient temperatures show the open form in the **O** state for both analogues (Fig. 12a–b) [11]. For this purpose, it was critical to employ relatively weak hydrogen bond donating groups to prevent the conformational switch before the redox interconversion to the **SQ** state. The systems in the **SQ** state equipped with hydrogen bond donating groups could experience the stabilization of the redox-active sites via hydrogen bonding. This intramolecular stabilization should only occur in the closed form, therefore, changes of the redox properties indicated by the CV and SWV served as an indirect evidence of the conformational lock by hydrogen bonding upon redox interconversion (Fig. 9). This indication was complemented by the UV-Vis-NIR spectroelectrochemical analysis of the conformational changes, where the hypo-hypsochromic shift of the quinoxaline absorption domain occurred only for the unprotected pyrrole-based **4** (Fig. 12c–d). Finally, the paramagnetic nature of the triplet **SQ** states can be utilized as a complementary tool in the evaluation of the geometry. The through-space dipole-dipole interaction of the two unpaired electron spins results in Zero Field Splitting (ZFS) [129,133,152,153], which can be characterized by the *D* and *E* parameters [133]. Since the *D* parameter is dependent on the distance between the spins, it offers a distinction

between the two conformations (Table 2). Analysis of the ZFS tensors [133-134] gives an estimate of the distance between the sites of the two unpaired electrons of 10.0 ± 0.5 Å (for instance, **1** and **3**), which is in excellent agreement with the distance between the two quinone walls in the closed conformation. The structure of closed **3** in **Q** state optimized by DFT calculations at the B3LYP/6-31G(d) level of theory shows a distance of 9.9 Å, whereas a distance of 9.4 Å was observed in the crystal structure with 1,4-dithiane as guest molecule encapsulated in the closed form (Fig. 13) [10,15,37]. The distance between the walls is slightly shorter upon encapsulation to enable establishment of close host-guest contacts. On the contrary, these distances are approximately 12–13 Å in the open form. These values are in agreement within the level of uncertainty of the EPR estimation and provide verification for the gripper-like conformational change in the triplet **SQ** dianions. However, the conformational change occurred even in the absence of hydrogen bond donating groups. Therefore, in order to probe the role of hydrogen bonding in the process, assessment of the binding properties was required, since preorganization to the closed form would result in the enhancement of the binding properties [4,15,16].

3.2.5. Binding Properties: Cyclic/Square-Wave Voltammetry and NMR Spectroscopy

Molecular grippers can bind smaller guest molecules inside their cavity and these binding properties are expressed through the association constants (K_a) that can be assessed by using different methods, such as NMR spectroscopy or cyclic/square-wave voltammetry. The binding occurs in the closed form and the binding affinities are hence determined by the kite→vase transition. It has been shown that the ΔG_{298K} for the vase→kite switch of **1-Q** is 1.8 kcal/mol in THF, whereas the corresponding ΔG_{298K} of **1-HQ** is 1.3 kcal/mol [4,15]. Furthermore, the K_a of complexes of **3-Q** are shown to be higher than those of **3-HQ**, which is assumed to be the result of lower $\Delta G_{298\ K}$ for the kite→vase switching process, in analogy to **2-Q**/**2-HQ** [15]. Accordingly, we can deduce that the more favorable kite→vase transition in the **SQ** state would result in higher binding affinities in this redox state.

We thereby compared binding of triptycene-based gripper **3** in three different redox states with several guest molecules, namely: cyclohexane, 1,4-dioxane, 1,4-dithiane, piperazine, and 1,4-cyclohexadione [4,15,16,37]. The binding properties of **3** in the **Q** and **HQ** state were investigated by ^{1}H NMR spectroscopy at ambient temperature by using mesitylene-d_{12}, which is commonly employed in this context as a noncompeting (since too large in size to occupy the vase cavity) solvent. The K_a were determined by using the concentrations of the species in solution. All the concentrations were estimated based on the concentration of an internal reference that acts as a noncompeting guest, most commonly 1,3,5-trimethoxybenzene. Binding constants K_a can be calculated based on the equation (2).

$$K_a = \frac{[\mathrm{HG}]}{[\mathrm{H}][\mathrm{G}]} \quad (2)$$

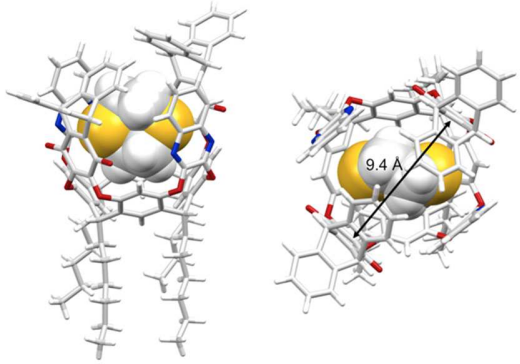

Fig. 13. Crystal structure of **3** in the **Q** state (*P*–1 space group) with a guest molecule (1,4-dithiane). Adapted with permission from ref. [11]. Copyright 2016 American Chemical Society.

The concentrations of the host [H] (eq. 3) and the guest [G] can be calculated from the differences between the initial concentrations and the concentration of the host-guest complex [HG] via equations (3) and (4). The concentration of the [HG] is calculated from the signal integral ratio between the ^{1}H NMR host-guest signals, corresponding to the encapsulated guest in the negative domain of the NMR spectrum, and the internal standard signals.

$$[\mathrm{H}] = [\mathrm{H}]_0 - [\mathrm{HG}] \quad (3)$$

$$[\mathrm{G}] = [\mathrm{G}]_0 - [\mathrm{HG}] \quad (4)$$

It is important to note that for the calculation of the K_a it is commonly accepted that only the concentrations corresponding to the certain degree of association (p), defined by equation (5), are considered, specifically those between 0.2–0.8 [154,155].

$$p = \frac{[\mathrm{HG}]}{[\mathrm{H}]_0} \quad (5)$$

The binding properties of the triptycene-based gripper **3** in the **SQ** state was probed via CV and SWV at ambient temperature by using CH_2Cl_2 as a solvent. Experiments were performed in solutions of CH_2Cl_2 containing 0.1 M *n*-Bu_4NBF_4 as a supporting electrolyte at 298 K and using scan rates of 100 mVs^{-1}. Potential shifts upon titration with different guest concentrations are used to calculate the K_a values by using the square potential scheme (Fig. 14). This approach enables to estimate the binding constants in the reduced states (K^-) relatively to the constants in the oxidized state (K^o) [22,37,156]. It is worth noting that CH_2Cl_2 is a competing solvent, which might result in obtaining lower value estimates for the K_a value. Moreover, to exclude other effects on the potential shifts, control experiments were performed in which the

cavitand wall models (such as **7**) were treated with the most prominent guests of our interest (i.e. dioxane or 1,4-dithiane). Consequently, the guests that demonstrated significant effects on the potential shifts of the model compounds (such as 1,4-piperazine due to hydrogen bonding) were excluded from the analysis.

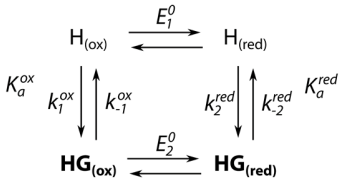

Fig. 14. Square electrochemical scheme [22,156].

Potential shifts of the first 2*e*⁻ reduction for **3** titrated with different concentrations of the corresponding guest molecules were used to estimate the guest binding constants (K^-) in the **SQ** state. For this purpose, two equations, (6) and (7), were employed to fit the data. Equation (6) was adapted from the literature, while the K^0 were obtained from ^{1}H NMR titrations in mesitylene-d_{12} [118].

$$\Delta E_{1/2} = E_{1/2(bound)} - E_{1/2(free)} = \frac{RT}{zF} ln\left(\frac{1+K^-[G]}{1+K^0[G]}\right) \qquad (6)$$

If we assume a weak binding in the neutral state, as indicated by the ^{1}H NMR experiments in CD_2Cl_2 where no binding was observed due to competitive guest binding, a simplified equation (7) can be used to obtain K^- [156].

$$\Delta E_{1/2} = E_{1/2(bound)} - E_{1/2(free)} = \frac{RT}{zF} ln(K^-[G]) \qquad (7)$$

Furthermore, a 2*e*⁻ transfer, as confirmed by RDV, and temperature of 298 K can be assumed for the fit.

For example, the fits for binding studies of **3** with 1,4-dioxane are shown in Fig. 15, whereas binding constants are summarized in Table 4. The K_a values were higher in the **SQ** state, while each of the three redox states (**Q**, **SQ**, and **HQ**) demonstrated different binding properties (Table 4). This behavior in the **SQ** state can be ascribed to its preorganized closed conformation that is likely to occur owing to stronger electrostatic interactions with the neighboring walls in the bis(radical anion) state. In this regard, systems stabilized by hydrogen bonding are expected to feature even stronger binding affinities.

To probe this effect, we studied binding of triptycene-based pyrrole-equipped gripper **5**, which adopts a closed conformation in the **SQ** state and features pyrrole hydrogen bond donating groups interacting with the reduced quinone walls, contributing to the binding enhancement [11,16]. Since the size of the cavity of the gripper appears well suited for binding small six-member-ringed molecules, as demonstrated by the crystal structure of the cavitand **3** with an encapsulated 1,4-dithiane guest molecule (Fig. 13) [11,16], we focused on this representative example. The binding ability of **5** for 1,4-dithiane in the **Q** state (K_a = 2.10 × 10³ M⁻¹) was higher by an order of magnitude compared to the reference **3** without hydrogen bond donating groups (1.27 × 10² M⁻¹) [11,16]. The binding was further enhanced in the **SQ** state (K_a > 2.10 × 10³ M⁻¹) [156]. Such binding enhancement is complementary to the characteristics of the gripper-like switch and it further emphasizes the role of hydrogen bonding in the process.

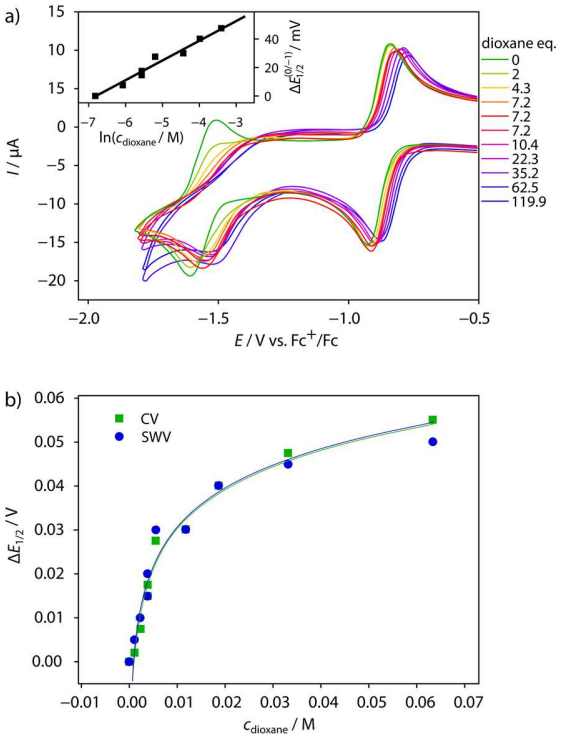

Fig. 15. Example of (a) a CV and (b) recorded potential shifts of a 0.5 mM cavitand **3** in 0.2 M *n*-Bu_4NBF_4 solution of dry CH_2Cl_2 upon titration with 1,4-dioxane at ambient temperature and a scan rate of 100 mVs⁻¹. Adapted with permission from ref. [11]. Copyright 2016 American Chemical Society.

Table 4. Binding constants of **3** in **Q** (K_a^Q, M⁻¹), **HQ** (K_a^{HQ}, M⁻¹), and **SQ** (K_a^{SQ}, M⁻¹) states. Adapted with permission from ref. [11].

Guest	K_a^Q, M⁻¹ [a]	K_a^{SQ}, M⁻¹ [b]	K_a^{HQ}, M⁻¹ [a]
	15 [15]	> 15 (51[c])	3.1 [15]
	4	949	< 0.1
	127	> 127 (399 [c])	40
	42	-[d]	< 0.1
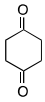	18	180	< 1

[a] K_a values were determined by ^{1}H NMR spectroscopy. Errors in K_a values are estimated to be 20% [15]. [b] K_a values were determined by CV / SWV [22,147,156]. [c] Simulation is recommended to quantify the K_a with more certainty since in the same order as in the oxidized states [156]. [d] Influence of hydrogen bonding cannot be directly excluded.

In summary, the demonstration of the redox switch accompanied by the conformational change of these systems in the **SQ** state, which is enhanced by hydrogen bonding, serves as an illustration of the potential for molecular gripping, opening the way to many possibilities towards future applications in molecular nanotechnology.

4. Conclusion and Outlook

A systematic overview of the redox chemistry of quinones is presented and applied on the study of controlling and monitoring quinone-based photoredox-switchable molecular grippers. These are based on resorcin[4]arene cavitands equipped by **Q** walls that mimic the ubiquinone environment of a photosynthetic reaction center, where the reduction to the **SQ** state affects the molecular machinery mediated by enhanced hydrogen bonding. The redox properties were thoroughly assessed by means of cyclic, rotating disc, and square-wave voltammetry, as well as by the analysis of model systems representing single cavitand walls. The **SQ** states were further characterized by UV-Vis-NIR spectroelectrochemistry, EPR, and ^{1}H ENDOR spectroscopy, which was complemented by NMR spectroscopy in the **Q** state. This enabled identifying the spectroscopic signatures, assessing the role of hydrogen bonding, as well as revealing the changes in geometry accompanying the redox switch.

This analysis based on a combination of electrochemical and spectroscopic techniques identified promising gripper candidates with respect to their conformational and redox properties. It was further demonstrated that conformational change occurred upon redox interconversion of grippers to the paramagnetic **SQ** radical anion state. Consequently, the conformational switch was accompanied by an enhancement in the binding properties, as demonstrated by NMR spectroscopy in the **Q** and cyclic/square-wave voltammetry in the **SQ** state. Moreover, presence of the hydrogen bond donating pyrrole groups resulted in further enhancement of the binding properties, highlighting the potential for molecular gripping. The study delivers a toolbox relevant to controlling and monitoring of quinone-based photoredox-switchable grippers that opens perspectives for the development of other molecular machines and devices based on this concept.

Corresponding authors

Email: diederich@org.chem.ethz.ch, lruhlman@unistra.fr

Acknowledgments

J.V.M. and F.D. are grateful to Swiss National Science Foundation Grant 200020_159802. L.R. and C. B. thank CNRS, the Université de Strasbourg (France). L.R. also thank the Université de Strasbourg for the projet "Idex Attractivité 2012" as well as the Labex CSC (Chemistry of Complex Systems), which has also supported one part of this research. M.Z. acknowledges the financial support of Slovak Research and Development Agency (APVV-15-0053) and Slovak Scientific Grant Agency VEGA (1/0416/17, 1/0466/18). The authors acknowledge the support of the colleagues involved in the research reviewed in this article.

Reference

[1] J.R. Moran, S. Karbach, D.J. Cram, Cavitands: Synthetic Molecular Vessels, J. Am. Chem. Soc. 104 (1982) 5826–5828.
[2] D.J. Cram, S. Karbach, H.-E. Kim, C.B. Knobler, E.F. Maverick, J.L. Ericson, R.C. Helgeson, Host-Guest Complexation. 46. Cavitands as Open Molecular Vessels Form Solvates, J. Am. Chem. Soc. 110 (1988) 2229–2237.
[3] V.A. Azov, A. Beeby, M. Cacciarini, A.G. Cheetham, F. Diederich, M. Frei, J.K. Gimzewski, V. Gramlich, B. Hecht, B. Jaun, T. Latychevskaia, A. Lieb, Y. Lill, F. Marotti, A. Schlegel, R.R. Schlittler, P.J. Skinner, P. Seiler, Y. Yamakoshi, Resorcin[4]arene Cavitand-Based Molecular Switches, Adv. Funct. Mater. 16 (2006) 147–156.
[4] I. Pochorovski, F. Diederich, Development of Redox-Switchable Resorcin[4]arene Cavitands, Acc. Chem. Res. 47 (2014) 2096–2105.
[5] F. Hof, S.L. Craig, C. Nuckolls, J. Rebek Jr., Molecular Encapsulation, Angew. Chem. Int. Ed. 41 (2002) 1488–1508.
[6] L. Pirondini, E. Dalcanale, Molecular Recognition at the Gas-Solid Interface: A Powerful Tool for Chemical Sensing, Chem. Soc. Rev. 36 (2007) 695–706.
[7] M. Melegari, M. Suman, L. Pirondini, D. Moiani, C. Massera, F. Ugozzoli, E. Kalenius, P. Vainiotalo, J.-C. Mulatier, J.-P. Dutasta, E. Dalcanale, Supramolecular Sensing with Phosphonate Cavitands, Chem. Eur. J. 14 (2008) 5772–5779.
[8] E. Biavardi, M. Favazza, A. Motta, I.L. Fragalà, C. Massera, L. Prodi, M. Montalti, M. Melegari, G.G. Condorelli, E. Dalcanale, Molecular Recognition on a Cavitand-Functionalized Silicon Surface, J. Am. Chem. Soc. 131 (2009) 7447–7455.
[9] Y. Yamakoshi, R.R. Schlittler, J.K. Gimzewski, F. Diederich, Synthesis of Molecular-Gripper-type Dynamic Receptors and STM-imaging of Self-Assembled Monolayers on Gold, J. Mater. Chem. 11 (2001) 2895–2897.
[10] I. Pochorovski, M.-O. Ebert, J.-P. Gisselbrecht, C. Boudon, W.B. Schweizer, F. Diederich, Redox-Switchable Resorcin[4]arene Cavitands: Molecular Grippers, J. Am. Chem. Soc. 134 (2012) 14702–14705.
[11] J. Milić, M. Zalibera, I. Pochorovski, N. Trapp, J. Nomrowski, D. Neshchadin, L. Ruhlmann, C. Boudon, O.S. Wenger, A. Savitsky, W. Lubitz, G. Gescheidt, F. Diederich, Paramagnetic Molecular Grippers: The Elements of Six-State Redox Switches, J. Phys. Chem. Lett. 7 (2016) 2470–2477.
[12] J. Milić, M. Zalibera, D. Talaat, J. Nomrowski, N. Trapp, L. Ruhlmann, C. Boudon, O.S. Wenger, A. Savitsky, W. Lubitz, F. Diederich, Photoredox-Switchable Resorcin[4]arene Cavitands: Radical Control of Molecular Gripping Machinery via Hydrogen Bonding, Chem. Eur. J. 24 (2018) 1431–1440.
[13] P.J. Skinner, A.G. Cheetham, A. Beeby, V. Gramlich, F. Diederich, Conformational Switching of Resorcin[4]arene Cavitands by Protonation, Helv. Chim. Acta 84 (2001) 2146–2153.

[14] M. Frei, F. Marotti, F.O. Diederich, Zn^{II}-induced Conformational Control of Amphiphilic Cavitands in Langmuir Monolayers, Chem. Commun. (2004) 1362–1363.
[15] I. Pochorovski, C. Boudon, J.-P. Gisselbrecht, M.-O. Ebert, W.B. Schweizer, F. Diederich, Quinone-based, Redox-Active Resorcin[4]arene Cavitands, Angew. Chem. Int. Ed. 51 (2012) 262–266.
[16] I. Pochorovski, J. Milić, D. Kolarski, C. Gropp, W.B. Schweizer, F. Diederich, Evaluation of Hydrogen-Bond Acceptors for Redox-Switchable Resorcin[4]arene Cavitands, J. Am. Chem. Soc. 136 (2014) 3852–3858.
[17] O.B. Berryman, A.C. Sather, J. Rebek Jr., A Light Controlled Cavitand Wall Regulates Guest Binding, Chem. Commun. 47 (2011) 656–658.
[18] V. García-López, J.V. Milić, M. Zalibera, D. Neshchadin, M. Kuss-Petermann, L. Ruhlmann, J. Nomrowski, N. Trapp, C. Boudon, G. Gescheidt, O.S. Wenger, F. Diederich, Light-Actuated Resorcin[4]arene Cavitands, Tetrahedron (2018), 74, 5615–5626.
[19] M. Frei, F. Diederich, R. Tremont, T. Rodriguez, L. Echegoyen, Tetrathiafulvalene (TTF)-Bridged Resorcin[4]arene Cavitands: Towards New Electrochemical Molecular Switches, Helv. Chim. Acta 89 (2006) 2040–2057.
[20] M.H. Düker, F. Kutter, T. Dülcks, V.A. Azov, Calix[4]arenes with 1,2- and 1,3-Upper Rim Tetrathiafulvalene Bridges, Supramol. Chem. 26 (2014) 552–560.
[21] S. Ruiz-Botella, P. Vidossich, G. Ujaque, C. Vicent, E. Peris, A Tetraferrocenyl-Resorcinarene Cavitand as a Redox-Switchable Host of Ammonium Salts, Chem. Eur. J. 21 (2015) 10558–10565.
[22] M. Gómez-Kaifer, P.A. Reddy, C.D. Gutsche, L. Echegoyen, Electroactive Calixarenes. 1. Redox and Cation Binding Properties of Calixquinones, J. Am. Chem. Soc. 116 (1994) 3580–3587.
[23] P.S. Guin, S. Das, P.C. Mandal, Electrochemical Reduction of Quinones in Different Media: A Review, Int. J. Electrochem. Article ID: 816202 (2011) 1–22.
[24] Y.-O. Kim, Y.M. Jung, S.B. Kim, B.H. Hong, K.S. Kim, S.-M. Park, Mechanistic Study on Electrochemical Reduction of Calix[4]quinone in Acetonitrile Containing Water, J. Phys. Chem. B 108 (2004) 4927–4936.
[25] Z. Zhang, L. Huang, V.M. Shulmeister, Y.-I. Chi, K.K. Kim, L.-W. Hung, A.R. Crofts, E.A. Berry, S-H. Kim, Electron Transfer by Domain Movement in Cytochrome bc, Nature 392 (1998) 677–685.
[26] Y.N. Pushkar, J.H. Golbeck, D. Stehlik, H. Zimmermann, Asymmetric Hydrogen-Bonding of the Quinone Cofactor in Photosystem I Probed by ^{13}C-Labeled Naphthoquinones, J. Phys. Chem. B 108 (2004) 9439–9448.
[27] C. Teutloff, W. Hofbauer, S.G. Zech, M. Stein, R. Bittl, W. Lubitz, High-Frequency EPR Studies on Cofactor Radicals in Photosystem I, Appl. Magn. Res. 21 (2001) 363–379.
[28] S. Sinnecker, E. Reijerse, F. Neese, W. Lubitz, Hydrogen Bond Geometries from Electron Paramagnetic Resonance and Electron-Nuclear Double Resonance Parameters: Density Functional Study of Quinone Radical Anion-Solvent Interactions, J. Am. Chem. Soc. 126 (2004) 3280–3290.
[29] A. Rodenberg, M. Orazietti, M. Mosberger, C. Bachmann, B. Probst, R. Alberto, P. Hamm, Quinones as Reversible Electron Relays in Artificial Photosynthesis, ChemPhysChem 17 (2016) 1321–1328.
[30] D. Schweinfurth, M. Zalibera, M. Kathan, C. Shen, M. Mazzolini, N. Trapp, J. Crassous, G. Gescheidt, F. Diederich, Helicene Quinones: Redox-Triggered Chiroptical Switching and Chiral Recognition of the Semiquinone Radical Anion Lithium Salt by Electron Nuclear Double Resonance Spectroscopy, J. Am. Chem. Soc. 136 (2014) 13045–13052.
[31] J.V. Milić, T. Schneeberger, M. Zalibera, K.Z. Milowska, Q.K. Ong, N. Trapp, L. Ruhlmann, C. Boudon, C. Thilgen, F. Diederich, Thioether-Functionalized Quinone-Based Resorcin[4]arene Cavitands: Electroswitchable Molecular Actuators, Helv. Chim. Acta 2019, 102, e1800225.
[32] E. Reijerse, F. Lendzian, R. Isaacson, W. Lubitz, A Tunable General Purpose Q-band Resonator for CW and Pulse EPR/ENDOR Experiments with Large Sample Access and Optical Excitation, J. Magn. Res. 214 (2012) 237–243.
[33] E.L. Hahn, Spin Echoes, Phys. Rev. 80 (1950) 580–601.
[34] E.R. Davies, A New Pulse ENDOR Technique, Phys. Lett. 47A (1974) 1–2.
[35] A. Nalepa, K. Möbius, W. Lubitz, A. Savitsky, High-Field ELDOR-Detected NMR Study of a Nitroxide Radical in Disordered Solids: Towards Characterization of Heterogeneity of Microenvironments in Spin-Labeled Systems, J. Magn. Res. 242 (2014) 203–213.
[36] S. Stoll, A. Schweiger, EasySpin, a Comprehensive Software Package for Spectral Simulation and Analysis in EPR, J. Magn. Res. 178 (2006) 42–55.
[37] J. V. Milić, Photoredox-Switchable Molecular Grippers: Design, Synthesis, and Spectroscopic Investigation, Doctoral Dissertation No. 24470, ETH Zurich, Switzerland, 2017.
[38] J. Glover, J.F. Pennock, G.A.J. Pitt, T. W. Goodwin, Richard Alan Morton, R.A. Morton, Ed., Biochemistry of Quinones, Academic Press New York, NY, USA, 1965. pp. 409-442.
[39] A. Di Marco, M. Gaetani, P. Orezzi, B.M. Scarpinato, R. Silverstrini, M. Soldati, T. Dasdia, L. Valentini, "Daunomycin", a New Antibiotic of Rhodomycin Group, Nature 201 (1964) 706–707.
[40] P. Montalbini, Effect of Infection by Uromyces Phaseoli (Pers.) Wint. on Electron Carrier Quinones in Bean Leaves, Phys. Plant Pathol. 3 (1973) 437–441.
[41] Y. Iwamoto, I.L. Hansen, T.H. Porter, K. Folkers, Inhibition of Coenzyme Q_{10}-Enzymes, Succinoxidase, and NADH-Oxidase, by Adriamycin and Other Quinones Having Antitumor Activity, Biochim. Biophys. Res. Commun. 58 (1974) 633–638.
[42] E. Bachmann, E. Weber, G. Zbinden, Effects of Seven Anthracycline Antibiotics on Electrocardiogram and Mitochondrial Function of Rat Hearts, Agents Actions 5 (1975) 383–393.
[43] N.R. Bachur, S.L. Gordon, M.V. Gee, Anthracycline Antibiotic Augmentation of Microsomal Electron Transport and Free Radical Formation, Mol. Pharmacol. 13 (1977) 901–910.
[44] J. Goodman, P. Hochstein, Generation of Free Radicals and Lipid Peroxidation by Redox Cycling of Adriamycin and Daunomycin, Biochem. Biophys. Res. Commun. 77 (1977) 797–803.
[45] W.S. Thayer, Adriamycin Stimulated Superoxide Formation in Submitochondrial Particles, Chem.-Biol. Interactions 19 (1977) 265–278.
[46] J.W. Lown, S.-K. Sim, K.C. Majumdar, R.-Y. Chang, Strand Scission of DNA by Bound Adriamycin and Daunorubicin in the Presence of Reducing Agents, Biochem. Biophys. Res. Commun. 76 (1977) 705–710.
[47] G. Zbinden, E. Bachmann, C. Holderegger, Model Systems for Cardiotoxic Effects of Anthracyclines, Antibiot. Chemother. 23 (1978) 255–270.
[48] V.J. Ferrans, Overview of Cardiac Pathology in Relation to Antracycline Cardiotoxicity, Cancer Treat. Rep. 62 (1978) 955–961.
[49] J.W. Lown, G. Weir, Studies Related to Antitumor Antibiotics. Part XIV. Reactions of Mitomycin B with DNA, Can. J. Biochem. 56 (1978) 296–304.
[50] S.T. Crooke, S.D. Reich, Eds., Anthracyclines: Current Status and New Developments, New York: Academic Press, 1980.
[51] B. Kalyanaraman, E. Perez-Reyes, R.P. Mason, Spin-Trapping and Direct Electron Spin Resonance Investigations of the Redox Metabolism of Quinone Anticancer Drugs, Biochim. Biophys. Acta. 630 (1980) 119–130.

[52] C.C. Winterbourn, Evidence for the Production of Hydroxyl Radicals from the Adriamycin Semiquinone and H_2O_2, FEBS Lett. 136 (1981) 89–94.
[53] J.W. Lown, A.V. Joshua, J.S. Lee, Molecular Mechanisms of Binding and Single-Strand Scission of Deoxyribonucleic Acid by the Antitumor Antibiotics Saframycins A and C, Biochemistry 21 (1982), 419–428.
[54] D.A. Bates, C.C. Winterbourn, Deoxyribose Breakdown by the Adriamycin Semiquinone and H_2O_2: Evidence for Hydroxyl Radical Participation, FEBS Lett. 145 (1982) 137–142.
[55] H. Muhammed, T. Ramasarma, C.K.R. Kurup, Inhibition of Mitochondrial Oxidative Phosphorylation by Adriamycin, Biochim. Biophys. Acta 722 (1982) 43–50.
[56] J.W. Lown, H.-H. Chen, J.A. Plambeck, E.M. Acton, Further Studies on the Generation of Reactive Oxygen Species from Activated Anthracyclines and the Relationship to Cytotoxic Action and Cardiotoxic Effects, Biochem. Pharmacol. 31 (1982) 575–581.
[57] E.J.F. Demant, NADH Oxidation in Submitochondrial Particles Protects Respiratory Chain Activity Against Damage by Adriamycin-Fe^{3+}, Eur. J. Biochem. 137 (1983) 113–118.
[58] K.J.A. Davies, J.H. Doroshow, P. Hochstein, Mitochondrial NADH Dehydrogenase-Catalyzed Oxygen Radical Production by Adriamycin, and the Relative Inactivity of 5-Iminodaunorubicin, FEBS Lett. 153 (1983) 227–230.
[59] P.K. Dutta, J.A. Hutt, Resonance Raman Spectroscopic Studies of Adriamycin and Copper(II)-Adriamycin and Copper(II)-Adriamycin-DNA Complexes, Biochemistry 25 (1986) 691–695.
[60] E. Goormaghtigh, J.M. Ruysschaert, Anthracycline Glycoside-Membrane Interactions, Biochim. Biophys. Acta 779 (1984) 271–288.
[61] H. Nakashima, N. Yamamoto, Y. Inoue, S. Nakamura, Inhibition by Doxorubicin of Huma Immuno-Deficiency Virus (HIV) Infection and Replication In Vitro, J. Antibiot. 40 (1987) 396–399.
[62] R.L. Blankespoor, R. Hsung, D.L. Schutt, Electroreductive Cleavage of Substituted 9,10-Anthraquinones in 50% Aqueous THF Buffers: a pH-Dependent Process, J. Org. Chem. 53 (1988) 3032–3035.
[63] B.L. Trumpower, The Protonmotive Q Cycle. Energy Transduction by Coupling of Proton Translocation to Electron Transfer by the Cytochrome bc_1 Complex, J. Biol. Chem. 265 (1990) 11409–11412.
[64] M.Y. Okamura, G. Feher, Proton Transfer in Reaction Centers from Photosynthetic Bacteria, Annu. Rev. Biochem. 61 (1992) 861–896.
[65] E. Feinstein, E. Canaani, L.M. Weiner, Dependence of Nucleic Acid Degradation on In Situ Free-Radical Production by Adriamycin, Biochemistry 32 (1993) 13156–13161.
[66] A. Kumbhar, S. Padhye, D. Ross, Cytotoxic Properties of Iron-Hydroxynaphthoquinone Complexes in Rat Hepatocytes, BioMetals 9 (1996) 235–240.
[67] D. Barasch, O. Zipori, I. Ringel, I. Ginsburg, A. Samuni, J. Katzhendler, Novel Anthraquinone Derivatives with Redox-Active Functional Groups Capable of Producing Free Radicals by Metabolism: Are Free Radicals Essential for Cytotoxicity?, Eur. J. Med. Chem. 34 (1999) 597–615.
[68] A. Bartoszek, Metabolic Activation of Adriamycin by NADPH-Cytochrome P450 Reductase; Overview of Its Biological and Biochemical Effects, Acta Biochim. Pol. 49 (2002) 323–331.
[69] H. Beraldo, A. Garnier-Suillerot, L. Tosi, F. Lavelle, Iron(III)-Adriamycin and Iron(III)-Daunorubicin Complexes: Physicochemical Characteristics, Interaction with DNA, and Antitumor Activity, Biochemistry 24 (1985) 284–289.
[70] F.C. de Abreu, P.A. de L. Ferraz, M.O.F. Goulart, Some Applications of Electrochemistry in Biomedical Chemistry. Emphasis on the Correlation of Electrochemical and Bioactive Properties, J. Braz. Chem. Soc. 13 (2002) 19–35.
[71] E.J.F. Demant, P.K. Jensen, Destruction of Phosphilipids and Respiratory-Chain Activity in Pig-Heart Submitochondrial Particles Induced by an Adriamycin-Iron Complex, Eur. J. Biochem. 132 (1983) 551–556.
[72] D. Marchal, W. Boireau, J.M. Laval, J. Moiroux, C. Bourdillon, An Electrochemical Approach of the Redox Behavior of Water Insoluble Ubiquinones or Plastoquinones Incorporated in Supported Phospholipid Layers, Biophys. J. 72 (1997) 2679–2687.
[73] O. Nimz, F. Lendzian, C. Boullais, W. Lubitz, Influence of Hydrogen Bonds on the Electronic *g*-Tensor and ^{13}C-Hyperfine Tensors of ^{13}C-Labeled Ubiquinones - EPR and ENDOR Study, Appl. Magn. Res. 14 (1998) 255–274.
[74] O. Burghaus, M. Plato, M. Rohrer, K. Möbius, F. MacMillan, W. Lubitz, 3-mm High-Field EPR on Semiquinone Radical Anions $Q^{\bullet-}$ Related to Photosynthesis and on the Primary Donor $P^{\bullet+}$ and Acceptor $Q_A^{\bullet-}$ in Reaction Centers of *Rhodobacter Sphaeroides* R-26, J. Phys. Chem. 97 (1993) 7639–7647.
[75] P.R. Vennam, N. Fisher, M.D. Krzyaniak, D.M. Kramer, M.K. Bowman, A Caged, Destabilized, Free Radical Intermediate in the Q-Cycle, ChemBioChem 14 (2013) 1745–1753.
[76] (a) J. Q. Chambers, "Electrochemistry of Quinones," in *The Chemistry of Quinonoid Compounds*, S. Patai, Z. Rappoport, Eds., Vol. 1, Ch. 14, Wiley, New York, NY, USA, 1974, pp. 737–791. (b) J. Q. Chambers, "Electrochemistry of Quinones," in *The Chemistry of Quinonoid Compounds*, S. Patai, Z. Rappoport, Eds., Vol. 2, Ch. 12, , Wiley, New York, NY, USA, 1988, pp. 719–757.
[77] S.I. Bailey, I.M. Ritchie, A Cyclic Voltammetric Study of the Aqueous Electrochemistry of Some Quinones, Electrochim. Acta 30 (1985) 3–12.
[78] D.O. Wipf, K.R. Wehmeyer, R.M. Wightman, Disproportionation of Quinone Radical Anions in Protic Solvents at High pH, J. Org. Chem. 51 (1986) 4760–4764.
[79] G.M. Rao, J.W. Lown, J.A. Plambeck, Electrochemical Studies of Antitumor Antibiotics. III. Daunorubicin and Adriamycin, J. Electrochem. Soc. 125 (1978) 534–539.
[80] C. Molinier-Jumel, B. Malfoy, J.A. Reynaud, G. Aubel-Sadron, Electrochemical Study of DNA-Anthracyclines Interaction, Biochem. Biophys. Res. Commun. 84 (1978) 441–449.
[81] R.P. Baldwin, D. Packett, T.M. Woodcock, Electrochemical Behavior of Adriamycin at Carbon Paste Electrodes, Anal. Chem. 53 (1981) 540–542.
[82] E.N. Chaney Jr., R.P. Baldwin, Electrochemical Determination of Adriamycin Compounds in Urine by Preconcentration at Carbon Paste Electrodes, Anal. Chem. 54 (1982) 2556–2560.
[83] F.C. Anson, B. Epstein, A Chronocoulometric Study of the Adsorption of Anthraquinone Monosulfonate on Mercury, J. Electrochem. Soc. 115 (1968) 1155–1158.
[84] M.P. Soriaga, P.H. Wilson, A.T. Hubbard, C.S. Benton, Orientational Transitions of Aromatic Molecules Adsorbed on Platinum Electrodes, J. Electroanal. Chem. 142 (1982) 317–336.
[85] P. He, R.M. Crooks, L.R. Faulkner, Adsorption and Electrode Reactions of Disulfonated Anthraquinones at Mercury Electrodes, J. Phys. Chem. 94 (1990) 1135–1141.
[86] Y.-B. Shim, S.-M. Park, Spectroelectrochemical Studies of p-Benzoquinone Reduction in Aqueous Media, J. Electroanal. Chem. 425 (1997) 201–207.
[87] H. Park, M.-S. Won, C. Cheong, Y.-B. Shim, In-Situ ESR Detection of Radical Species of p-Benzoquinone in Aqueous Media, Electroanalysis 14 (2002) 1501–1507.
[88] R.J. Forster, J.P. O'Kelly, Protonation Reactions of Anthraquinone-2,7-disulphonic Acid in Solution and within Monolayers, J. Electroanal. Chem. 498 (2001) 127–135.
[89] Y. Tang, Y. Wu, Z. Wang, Spectroelectrochemistry for Electroreduction of p-Benzoquinone in Unbuffered Aqueous Solution, J. Electrochem. Soc. 148 (2001) E133–E138.
[90] M. Quan, D. Sanchez, M.F. Wasylkiw, D.K. Smith, Voltammetry of Quinones in Unbuffered Aqueous Solution: Reassessing the Roles of Proton Transfer and Hydrogen Bonding in the Aqueous Electrochemistry of Quinones, J. Am. Chem. Soc. 129 (2007) 12847–12856.

[91] O.H. Müller, Oxidation-Reduction Potentials Measured with the Dropping Mercury Electrode. III. Polarographic Study of Quinhydrone in Buffered and Unbuffered Solutions, J. Am. Chem. Soc. 62 (1940) 2434–2441.
[92] I.M. Kolthoff, E.F. Orlemann, The Use of the Dropping Mercury Electrode as an Indicator Electrode in Poorly Poised Systems, J. Am. Chem. Soc. 63 (1941) 664–667.
[93] J.C. Abbott, J.W. Collat, Indirect Polarographic Determination of Acids, Anal. Chem. 35 (1963) 859–863.
[94] R.T. Robertson, B.D. Pendley, Microelectrodes as Probes in Low Electrolyte Solutions: The Reduction of Quinone in Aqueous Sulfuric Acid Solution, J. Electroanal. Chem. 374 (1994) 173–177.
[95] Y. Sato, M. Fujita, F. Mizutani, K. Uosaki, Electrochemical Properties of the 2-Mercaptohydroquinone Monolayer on a Gold Electrode. Effect of Solution pH, Adsorption Time and Concentration of the Modifying Solution, J. Electroanal. Chem. 409 (1996) 145–154.
[96] P.H. Given, M.E. Peover, Polarographic Reduction of Aromatic Hydrocarbons and Carbonyl Compounds in Dimethylformamide in the Presence of Proton-Donors, J. Chem. Soc. (1960) 385–393.
[97] A. Capon, R. Parsons, The Rate of a Simple Electron Exchange Reaction as a Function of the Electrode Material, Electroanal. Chem. Interfacial Electrochem. 46 (1973) 215–222.
[98] R.D. Rieke, T. Saji, N. Kujundzic, Electrochemical Studies of Methyl Substituted 1,4-Quinones. Part I. The Electrochemical Dimerization of Duroquinone, J. Electroanal. Chem. 102 (1979) 397–405.
[99] M.D. Stallings, M.M. Morrison, D.T. Sawyer, Redox Chemistry of Metal-Catechol Complexes in Aprotic Media. 1. Electrochemistry of Substituted Catechols and Their Oxidation Products, Inorg. Chem. 20 (1981) 2655–2660.
[100] C. Russel, W. Jaenicke, Heterogeneous Electron Exchange of Quinones in Aprotic Solvents. Part III. The Second Reduction Step of p-Benzoquinone and Its Dependence on the Supporting Electrolyte, J. Electroanal. Chem. 199 (1986) 139–151.
[101] M. Oyama, T. Hoshino, S. Okazaki, Solvent Effect on the Ion Pair Formation Between 2,3,5,6-Tetrachloro-1,4-benzoquinone Anion Radical and Mg^{2+} Measured Using a Pulse Electrolysis Stopped Flow Method, J. Electroanal. Chem. 401 (1996) 243–246.
[102] M. Oyama, F. Marken, R.D. Webster, J.A. Cooper, R.G. Compton, S. Okazaki, Ion Pair Formation Between the Electrogenerated 2,3-Dichloro-5,6-dicyano-1,4-benzoquinone Dianion and the Sodium Ion at Platinum Surfaces, J. Electroanal. Chem. 451 (1998) 193–201.
[103] S.U. Pedersen, T.B. Christensen, T. Thomasen, K. Daasbjerg, New Methods for the Accurate Determination of Extinction and Diffusion Coefficients of Aromatic and Heteroaromatic Radical Anions in *N,N*-Dimethylformamide, J. Electroanal. Chem. 454 (1998) 123–143.
[104] M. Aguilar-Martínez, G. Cuevas, M. Jiménez-Estrada, I. González, B. Lotina-Hennsen, N. Macías-Ruvalcaba, An Experimental and Theoretical Study of the Substituent Effects on the Redox Properties of 2-[(R-phenyl)amine]-1,4-naphthalenediones in Acetonitrile, J. Org. Chem. 64 (1999) 3684–3694.
[105] M. Shamsipur, A. Siroueinejad, B. Hemmateenejad, A. Abbaspour, H. Sharghi, K. Alizadeh, S. Arshadi, Cyclic Voltammetric, Computational, and Quantitative Structure–Electrochemistry Relationship Studies of the Reduction of Several 9,10-Anthraquinone Derivatives, J. Electroanal. Chem. 600 (2007) 345–358.
[106] M.W. Lehmann, D.H. Evans, Anomalous Behavior in the Two-Step Reduction of Quinones in Acetonitrile, J. Electroanal. Chem. 500 (2001) 12–20.
[107] S. Hayano, M. Fujihira, The Effect of Water on the Reduction Potentials of Some Aromatic Compounds in the DMF-Water System, Bull. Chem. Soc. Jpn. 44 (1971) 2051–2055.
[108] M. Gómez, F.J. González, I. González, A Model for Characterization of Successive Hydrogen Bonding Interactions with Electrochemically Generated Charged Species. The Quinone Electroreduction in the Presence of Donor Protons, Electroanalysis 15 (2003) 635–645.
[109] M. Gómez, F.J. González, I. González, Effect of Host and Guest Structures on Hydrogen Bonding Association: Influence of Stoichiometry and Equilibrium Constants, J. Electrochem. Soc. 150 (2003) E527–E534.
[110] I.M. Kolthoff, T.B. Reddy, Polarography and Voltammetry in Dimethylsulfoxide, J. Electrochem. Soc. 108 (1961) 980–985.
[111] N. Gupta, H. Linschitz, Hydrogen-Bonding and Protonation Effects in Electrochemistry of Quinones in Aprotic Solvents, J. Am. Chem. Soc. 119 (1997) 6384–6391.
[112] M.F. Marcus, M.D. Hawley, Electrochemical Studies of the Redox Behavior of α-Tocopherylquinone and a Related Model Quinone, Biochim. Biophys. Acta. 222 (1970) 163–173.
[113] A.C. Aten, C. Büthker, G.J. Hoijtink, Electron Transfer to Aromatic Hydrocarbons at the Dropping Mercury Electrode, Trans. Faraday Soc. 55 (1959) 324–330.
[114] V. Glezer, J. Stradins, J. Freimanis, L. Baider, The Mechanism of Electrochemical Reduction of Intramolecular Charge-Transfer Complexes Derived from 1,4-Naphthoquinone, Electrochim. Acta. 28 (1983) 87–95.
[115] M. Oyama, K. Nozaki, S. Okazaki, Pulse-Electrolysis Stopped-Flow Method for the Electrospectroscopic Analysis of Short-Lived Intermediates Generated in the Electrooxidation of Triphenylamine, Anal. Chem. 63 (1991) 1387–1392.
[116] P.A. Reddy, C.D. Gutsche, Calixarenes. 32. Reactions of Calix[4]quinones, J. Org. Chem. 58 (1993) 3245–3251.
[117] S. Thulasi, J. Babu, A. Babukuttannair, V. Sreemathi, R.L. Varma, Direct Access to Upper Rim Substituted Mono- and Diaryloxy Calix[4]arenes via Bis(spirodienone) Route, Tetrahedron 66 (2010) 5270–5276.
[118] A.H. Flood, A.E. Kaifer, Supramolecular Electrochemistry in Supramolecular Chemistry: From Molecules to Nanomaterials, Vol 2, P. A. Gale, J. W. Steed, Eds., Wiley, Chichester, 2012, pp. 451–472.
[119] M. Oyama, R.D. Webster, M. Suárez, F. Marken, R.G. Compton, S. Okazaki, Mechanistic Aspects of the Electrochemical Reduction of 7,7,8,8-Tetracyanoquinodimethane in the Presence of Mg^{2+} or Ba^{2+}, J. Phys. Chem. B 102 (1998) 6588–6595.
[120] P.D. Beer, Z. Chen, P.A. Gale, Diester-Calix[4]arenediquinone Complexation and Electrochemical Recognition of Group 1 and 2, Ammonium and Alkyl Ammonium Guest Cations, Tetrahedron 50 (1994) 931–940.
[121] D. Choi, T.D. Chung, S.K. Kang, S.K. Lee, T. Kim, S.-K. Chang, H. Kim, Electrochemical Recognition of Ammonium and Alkali Metal Cations with Calix[4]arenediquinone, J. Electroanal. Chem. 387 (1995) 133–134.
[122] T.D. Chung, D. Choi, S.K. Kang, S.K. Lee, S.-K. Chang, H. Kim, Electrochemical Behavior of Calix[4]arenediquinones and Their Cation Binding Properties, J. Electroanal. Chem. 396 (1995) 431–439.
[123] K. Pekmez, M. Can, A. Yildiz, Electrochemistry in Aprotic Solvents Containing Anhydrous Perchloric Acid: Electroreduction Behavior of Quinones, Electrochim. Acta 38 (1993) 607–611.
[124] W. Kaim, J. Fiedler, Spectroelectrochemistry: The Best of Two Worlds, Chem. Soc. Rev. 38 (2009) 3373–3782.
[125] J. Bonin, M. Routier, Transient Absorption Spectroscopy Studies of Proton-Coupled Electron Transfers, Artificial Photosynthesis 1 (2013) 6–15.
[126] T.N.V. Karsili, D. Tuna, J. Ehrmaier, W. Domcke, Photoinduced Water Splitting via Benzoquinone and Semiquinone Sensitisation, Phys. Chem. Chem. Phys. 17 (2015) 32183–32193.
[127] N. Vân Anh, R.M. Williams, Bis-Semiquinone (Bi-Radical) Formation by Photoinduced Proton Coupled Electron Transfer in Covalently Linked Catechol–Quinone Systems: Aviram's

Hemiquinones Revisited, Photochem. Photobiol. Sci. 11 (2012) 957–961.
[128] J. Yuasa, S. Yamada, S. Fukuzumi, Direct EPR Detection of a Hydrogen-Bonded Complex between a Semiquinone Radical Anion and a Protonated Amino Acid, and Electron Transfer Driven by Hydrogen Bonding, Angew. Chem. Int. Ed. 46 (2007) 3553–3555.
[129] R. Calvo, E.C. Abresch, R. Bittl, G. Feher, W. Hofbauer, R.A. Isaacson, W. Lubitz, M.Y. Okamura, M.L. Paddock, EPR Study of the Molecular and Electronic Structure of the Semiquinone Biradical $Q_A^{-\bullet}Q_B^{-\bullet}$ in Photosynthetic Reaction Centers from *Rhodobacter sphaeroides*, J. Am. Chem. Soc. 122 (2000) 7327–7341.
[130] J. Hankache, D. Hanss, O.S. Wenger, Hydrogen-Bond Strengthening upon Photoinduced Electron Transfer in Ruthenium–Anthraquinone Dyads Interacting with Hexafluoroisopropanol or Water, J. Phys. Chem. A 116 (2012) 3347–3358.
[131] M.P. Bubnov, I.A. Teplova, V.K. Cherkasov, G.A. Abakumov, EPR Study of o-Semiquinone-Catecholate Cobalt Complexes with Bis(diphenylphosphanyl)ethane, Eur. J. Inorg. Chem. (2003) 2519–2523.
[132] T. Takui, K. Sato, D. Shiomi, K. Itoh, T. Kaneko, E. Tsuchida, H. Nishide, FT Pulsed ESR/Electron Spin Transient Nutation (ESTN) Spectroscopy Applied to High-Spin Systems in Solids; Direct Evidence of a Topologically Controlled High-Spin Polymer as Models for Quasi ID Organic Ferro-and Superpara-Magnets, Mol. Crys. Liq. Cryst. 279 (1996) 155–176.
[133] M.L. Munzrova, DFT Calculations of EPR Hyperfine Coupling Tensors, in Calculation of NMR and EPR Parameters. Theory and Applications, M. Kaupp, M. Bühl, V.G. Malkin, Eds., Wiley-VCH, Weinheim, 2004, pp. 463–482.
[134] N. Cox, M. Retegan, F. Neese, D.A. Pantazis, A. Boussac, W. Lubitz, Electronic Structure of the Oxygen-Evolving Complex in Photosystem II Prior to O-O Bond Formation, Science 345 (2014) 804–808.
[135] A.E. Alegría, M. López, N. Guevara, Thermodynamics of Semiquinone Disproportionation in Aqueous Buffer, Faraday Trans. 92 (1996) 4965–4968.
[136] W.O. Feikema, P. Gast, I.B. Klenina, I.I. Proskuryakov, EPR Characterisation of the Triplet State in Photosystem II Reaction Centers with Singly Reduced Primary Acceptor Q_A, Biochim. Biophys. Acta 1709 (2005) 105–112.
[137] M. Flores, R. Isaacson, E. Abresch, R. Calvo, W. Lubitz, G. Feher, Protein-Cofactor Interactions in Bacterial Reaction Centers from *Rhodobacter sphaeroides* R-26: I. Identification of the ENDOR Lines Associated with the Hydrogen Bonds to the Primary Quinone Q_A^{-}, Biophys. J. 90 (2006) 3356–3362.
[138] E. Martin, R.I. Samoilova, K.V. Narasimhulu, T.-J. Lin, P.J. O'Malley, C.A. Wraight, S.A. Dikanov, Hydrogen Bonding and Spin Density Distribution in the Q_B Semiquinone of Bacterial Reaction Centers and Comparison with the Q_A Site, J. Am. Chem. Soc. 133 (2011) 5525–5537.
[139] E. Martin, A. Baldansuren, T.-J. Lin, R.I. Samoilova, C.A. Wraight, S.A. Dikanov, P.J. O'Malley, Hydrogen Bonding between the Q_B Site Ubisemiquinone and Ser-L223 in the Bacterial Reaction Center: A Combined Spectroscopic and Computational Perspective, Biochemistry 51 (2012) 9086–9093.
[140] M. Shanmugam, G. Xue, L. Que Jr., B.M. Hoffman, ^{1}H-ENDOR Evidence for a Hydrogen-Bonding Interaction That Modulates the Reactivity of a Nonheme Fe^{IV}═O Unit, Inorg. Chem. 51 (2012) 10080–10082.
[141] J.D. Megiatto Jr., D.D. Méndez-Hernández, M.E. Tejeda-Ferrari, A.-L. Teillout, M.J. Llansola-Portolés, G. Kodis, O.G. Poluektov, T. Rajh, V. Mujica, T.L. Groy, D. Gust, T.A. Moore, A.L. Moore, A Bioinspired Redox Relay that Mimics Radical Interactions of the Tyr–His Pairs of Photosystem II, Nat. Chem. 6 (2014) 423–428.
[142] A.T. Taguchi, P.J. O'Malley, C.A. Wraight, S.A. Dikanov, Hydrogen Bond Network around the Semiquinone of the Secondary Quinone Acceptor Q_B in Bacterial Photosynthetic Reaction Centers, J. Phys. Chem. B 119 (2015) 5805–5814.
[143] L. Favereau, A. Makhal, Y. Pellegrin, E. Blart, J. Petersson, E. Göransson, L. Hammarström, F. Odobel, A Molecular Tetrad That Generates a High-Energy Charge-Separated State by Mimicking the Photosynthetic Z-Scheme, J. Am. Chem. Soc. 138 (2016) 3752–3760.
[144] Y. Ge, L. Miller, T. Ouimet, D.K. Smith, Electrochemically Controlled Hydrogen Bonding. o-Quinones as Simple Redox-Dependent Receptors for Arylureas, J. Org. Chem. 65 (2000) 8831–8838.
[145] A.K. Turek, D.J. Hardee, A.M. Ullman, D.G. Nocera, E.N. Jacobsen, Activation of Electron-Deficient Quinones through Hydrogen-Bond-Donor-Coupled Electron Transfer, Angew. Chem. Int. Ed. 55 (2016) 539–544.
[146] Y. Kato, R. Nagao, T. Noguchi, Redox Potential of the Terminal Quinone Electron Acceptor Q_B in Photosystem II Reveals the Mechanism of Electron Transfer Regulation, Proc. Nat. Acad. Sci. USA 113 (2016) 620–625.
[147] P.L. Boulas, M. Gómez-Kaifer, L. Echegoyen, Electrochemistry of Supramolecular Systems, Angew. Chem. Int. Ed. 37 (1998) 216–247.
[148] D.M. Murphy, R.D. Farley, Principles and Applications of ENDOR Spectroscopy for Structure Determination in Solution and Disordered Matrices, Chem. Soc. Rev. 35 (2006) 249–268.
[149] H. Li, A.C. Fahrenbach, A. Coskun, Z. Zhu, G. Barin, Y.-L. Zhao, Y.Y. Botros, J.-P. Sauvage, J.F. Stoddart, A Light-Stimulated Molecular Switch Driven by Radical-Radical Interactions in Water, Angew. Chem. Int. Ed. 50 (2011) 6782–6788.
[150] A.C. Fahrenbach, Z. Zhu, D. Cao, W.-G. Liu, H. Li, S.K. Dey, S. Basu, A. Trabolsi, Y.Y. Botros, W.A. Goddard III, J.F. Stoddart, Radically Enhanced Molecular Switches, J. Am. Chem. Soc. 134 (2012) 16275–16288.
[151] A. Trabolsi, N. Khashab, A.C. Fahrenbach, D.C. Friedman, M.T. Colvin, K.K. Cotí, D. Benítez, E. Tkatchouk, J.-C. Olsen, M.E. Belowich, R. Carmielli, H.A. Khatib, W.A. Goddard III, M.R. Wasielewski, J.F. Stoddart, Radically Enhanced Molecular Recognition, Nat. Chem. 2 (2010) 42–49.
[152] A. Caneschi, A. Dei, H. Lee, D.A. Shultz, L. Sorace, Ferromagnetically Coupled Bis(semiquinone) Ligand Enforces High-Spin Ground States in Bis-metal Complexes, Inorg. Chem. 40 (2001) 408–411.
[153] D.A. Shultz, R.M. Fico Jr., S.H. Bodnar, R.K. Kumar, K.E. Vostrikova, J.W. Kampf, P.D. Boyle, Trends in Exchange Coupling for Trimethylenemethane-Type Bis(Semiquinone) Biradicals and Correlation of Magnetic Exchange with Mixed Valency for Cross-Conjugated Systems, J. Am. Chem. Soc. 125 (2003) 11761–11771.
[154] K. Hirose, A Practical Guide for the Determination of Binding Constants, J. Inclusion Phenom. Macrocyclic. Chem. 39 (2001) 139–209.
[155] C. Schalley, Ed., Analytical Methods in Supramolecular Chemistry, Wiley-VCH, Weinheim, Germany, 2007.
[156] S.R. Miller, D.A. Gustowski, Z.-H. Chen, G.W. Gokel, L. Echegoyen, A.E. Kaifer, Rationalization of the Unusual Electrochemical Behavior Observed in Lariat Ethers and Other Reducible Macrocyclic Systems, Anal. Chem. 60 (1988) 2021–2024.

5. Graphical Abstract

Spectro-Electrochemical Toolbox for Monitoring and Controlling Quinone-Mediated Redox-Driven Molecular Gripping

Jovana V. Milić [a,b,#], Thomas Schneeberger [a,#], Michal Zalibera [c], François Diederich [a,*], Corinne Boudon [d], Laurent Ruhlmann [d*]

[a]*Laboratory of Organic Chemistry, ETH Zurich, HCI, Vladimir-Prelog-Weg 3, 8093 Zurich, Switzerland*
[b]*Laboratory of Photonics and Interfaces, EPFL, Station 6, 1015 Lausanne, Switzerland*
[c]*Institute of Physical Chemistry and Chemical Physics, Slovak University of Technology, Radlinského 9, 81237 Bratislava, Slovakia*
[d]*Université de Strasbourg, Laboratoire d'Electrochimie et de Chimie Physique du Corps Solide, Institut de Chimie de Strasbourg, UMR 7177, 4 rue Blaise Pascal, CS 90032, 67081 Strasbourg, France*